Received: 20 May 2025 | Revised: 1 July 2025 | Accepted: 22 July 2025 | Published online: 15 August 2025

REVIEW

Smart Wearable Technology
2025, Vol. 1, A8, 21 Pages
DOI: 10.47852/bonviewSWT52026191

BON VIEW PUBLISHING

Recent Advances in Flexible Perovskite Light-Emitting Diodes

Qi Han[1], Peng Han[1], Daizhe Wang[1,*] and Yong Zhang[1,2,*]

[1]*School of Materials Science and Engineering, Harbin Institute of Technology, China*

[2]*Zhengzhou Research Institute, Harbin Institute of Technology, China*

Abstract: Flexible perovskite light-emitting diodes (f-PeLEDs) have demonstrated their great potential for next-generation lighting and wearable display technologies due to their high color purity, excellent optoelectronic performance, solution processability, as well as their ultrathin and lightweight nature. Currently, the external quantum efficiency (EQE) and device stability of perovskite light-emitting diodes (PeLEDs) have been constantly updated in the past decade. However, limited by the inherent defect of perovskite and poor interfacial contact, the EQE of f-PeLEDs is still far lower than that of devices on rigid glass substrates. Therefore, it is necessary to provide an insightful summary to promote their further development. This review summarizes the strategies and the latest progress in improving the optoelectronic and mechanical performance of f-PeLEDs through the optimization of flexible substrates and electrodes, hole transport layers, perovskite layers, and fabrication techniques. Finally, this work summarizes and discusses the development and future challenges of flexible light-emitting diodes in the display field.

Keywords: perovskite light-emitting diodes, flexible light-emitting diodes, flexible substrates, transparent electrodes, hole transport layer engineering, defect passivation engineering

1. Introduction

With the advancement of modern display technology, the demand for flexible electronic products has grown rapidly [1, 2]. Currently, compared with traditional rigid light-emitting diodes (LEDs), flexible light-emitting diodes have been successfully applied in curved displays, curved smartphones, foldable handsets, and various wearable electronic products (such as health monitoring, biomedical devices, electronic skins) due to their excellent tolerance to curvilinear surfaces and mechanical deformation while maintaining high brightness under mechanical stress or deformation [3–11] (Figure 1 [12]).

Perovskite materials possess outstanding optoelectronic properties, including high electron/hole mobility, high photoluminescence quantum yield, high defect tolerance, high color purity, and tunable emission spectra [13–15]. Perovskite light-emitting diodes (PeLEDs) typically adopt a planar heterojunction (sandwich) structure, where the perovskite layer is embedded between the electron transport layer (ETL) and the hole transport layer (HTL) [16]. Depending on the relative arrangement of these charge transport layers, PeLEDs can be classified into the normal p-i-n structure and the inverted n-i-p structure (Figure 2(a) and (b)) [17]. In the normal structure, the HTL is located beneath the perovskite layer, whereas in the inverted structure, the ETL is positioned below the perovskite layer [18–20]. The working mechanism of PeLEDs involves the process in which, under forward bias conditions, electrons and holes are injected from the anode and cathode, respectively, and migrate through the ETL and HTL before being injected into the perovskite light-emitting layer [21]. Under the influence of Coulomb forces, excitons (electron-hole pairs) are formed, and the excitons release photons in all directions through radiative recombination [22]. Due to the good flexibility of perovskite materials, flexible electrodes and substrates could be used to replace the rigid substrates and electrodes of traditional PeLEDs to obtain f-PeLEDs [23]. The working mechanism of f-PeLEDs is the same as that of PeLEDs.

For f-PeLEDs, the external quantum efficiency (EQE) and stability are critical parameters for evaluating their optoelectronic and mechanical properties. EQE is defined as the ratio of the flux of emitted photons over the number of electrons injected into the device per unit time, expressed as:

$$\mathrm{EQE} = \frac{\text{photons emitted into free space}}{\text{charges injected into the emitter film}} = \eta_{inj} \times \eta_{rad} \times \eta_{out} \tag{1}$$

It is determined by the injection efficiency (η_{inj}), radiative recombination efficiency (η_{rad}), and outcoupling efficiency (η_{out}). η_{inj} describes the quantity of charge carriers injected into the perovskite layer through electrodes, η_{rad} refers to the ratio of radiatively recombined excitons to the total excitons

*Corresponding authors: Daizhe Wang, School of Materials Science and Engineering, Harbin Institute of Technology, China. Email: daizhewang@hit.edu.cn and Yong Zhang, School of Materials Science and Engineering, Harbin Institute of Technology and Zhengzhou Research Institute, Harbin Institute of Technology, China. Email: yongzhang@hit.edu.cn

Figure 1
Future of flexible and wearable displays: (a) smart glasses or smart lens, (b) smart watch with wearable biosensors, (c) fabric display, (d) ultrathin electronic tattoo, (e) bendable and foldable display, and (f) transparent smart windows

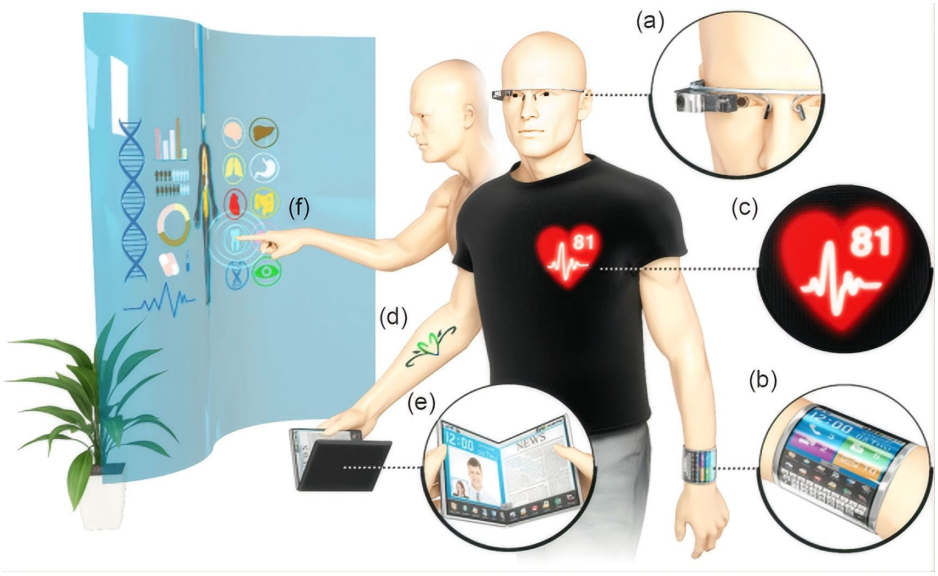

generated in the device, and η_{out} is determined by the optical losses originating from the waveguide and substrate modes caused the mismatched refractive indices between the different device layers, substrate, and air [24]. To enhance the device EQE, η_{inj} could be improved by achieving a balanced injection of electrons and holes. Defect passivation could effectively reduce the quenching effect of internal defects on excitons in the perovskite layer, thereby increasing the η_{rad}. Additionally, designing an optimized device structure could reduce optical losses and enhance the η_{out} [25]. The operational stability of the devices is judged by the Luminance Half-Life (T50) [26]. T50 is a core indicator for evaluating light-emitting devices. It refers to the time required for the initial luminance of a device to decay to 50% of its original luminance under constant current drive [27].

Currently, the EQEs of pure-green and pure-red PeLEDs based on rigid glass substrates have exceeded 30%, establishing them as ideal candidates for next-generation lighting and display technologies [28–30]. Unfortunately, PeLEDs based on glass substrates have poor mechanical flexibility and are prone to fracture under bending stress [31]. Consequently, the fabrication of flexible perovskite light-emitting diodes (f-PeLEDs) is based on flexible substrates [32]. Although f-PeLEDs have developed rapidly, the EQE of green f-PeLED without pattern has reached 22.1% and could still maintain 82% performance after 2000 cycles [33]. Meanwhile, the EQE of red f-PeLED has reached 16.2%, and the device could withstand folding up to 5000 times without significant degradation [34]. In contrast, the EQE of f-PeLEDs lags far behind that of rigid PeLEDs, which limits their application in flexible optoelectronics and displays [35, 36]. However, due to the high defect density of perovskite emission films, poor crystallinity of thin films, and the brittleness of polycrystalline perovskites, the luminescent performance and mechanical properties of f-PeLEDs still need to be further improved [33, 34]. To meet the practical application requirements of flexible devices, all functional layers of f-PeLEDs should have excellent mechanical properties (Figure 2(c)) [28]. To promote the application of f-PeLEDs in smart wearable devices and stretchable displays, large-scale fabrication is a prerequisite for solid-state drive and display applications [24, 37–39]. However, the development of high-performance large-area devices and suitable manufacturing processes remains a challenge [40–42].

Although the flexibility of f-PeLEDs mainly depends on the flexibility of the perovskite layer, all functional layers must exhibit excellent mechanical performance to fulfill the practical requirements of flexible electronic devices [42–44]. Therefore, developing flexible substrates, improving the electrical conductivity of flexible electrodes [45], and adjusting the HTL to better match the perovskite layer for promoting charge injection [46] are key strategies to enhance device stability and flexibility. Additionally, by optimizing the perovskite film to further achieve efficient f-PeLEDs [34], these approaches enhance both the mechanical robustness and optoelectronic performance of f-PeLEDs.

Herein, we aim to summarize the recent progress in f-PeLEDs from the perspective of device structure. As shown in Figure 2(d), we will first analyze the impact of flexible substrates and transparent electrodes on enhancing device performance, focusing on their compositional characteristics. Next, we investigate the optimization strategies for the widely used HTLs and explore criteria for selecting alternative hole transport materials suitable for f-PeLEDs. Additionally, we provide a comprehensive overview of the roles of additive engineering and composition engineering in improving the quality of perovskite films. Since the research on the ETL is relatively mature, the widely used material is TPBi [34, 47]. Subsequently, we describe the methodologies employed in fabricating perovskite functional layers. Finally, we highlight the remaining challenges facing f-PeLEDs and propose potential future directions.

2. Modification of Flexible Substrate and Electrode

PeLEDs based on an indium tin oxide (ITO) substrate as anode electrode have achieved a major breakthrough, with the EQE

Figure 2
(a) P-i-n and (b) n-i-p structure of PeLEDs; (c) device structure of f-PeLED; (d) strategies of enhancing the performance of f-PeLEDs

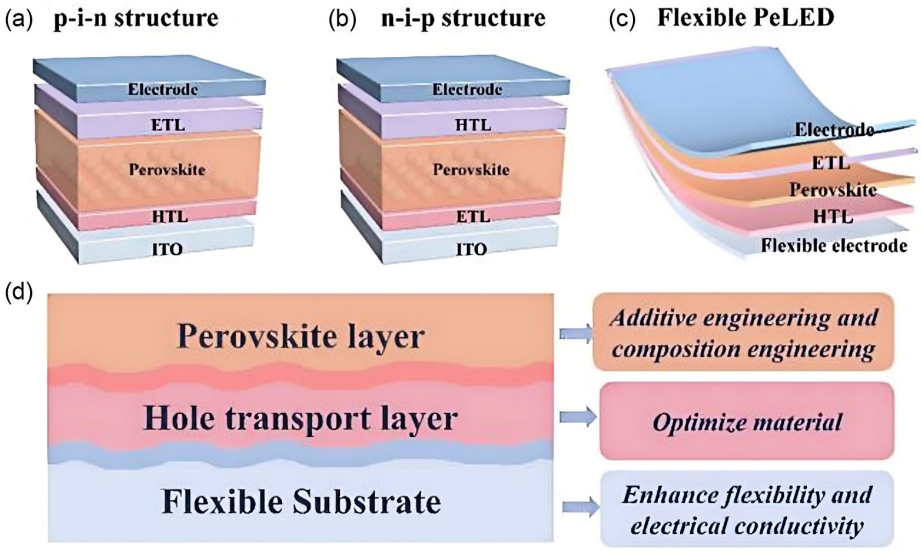

increasing from less than 1% to over 30% [48]. However, the highly brittle nature of glass substrates and ITO electrodes results in their limited bending resistance, which significantly affects the foldable property of f-PeLEDs [1]. Consequently, high mechanical stability flexible substrates and electrodes are considered as alternatives to traditional glass substrates and ITO electrodes in f-PeLEDs. Nevertheless, flexible substrates have lower optical transmittance than glass, and the high Young's modulus of ITO results in poor compatibility with flexible substrates [49]. In addition, it is difficult to achieve mechanically stable perovskite films that possess excellent optoelectronic properties on flexible substrates [28, 48, 50]. As a result, the performance of f-PeLEDs currently lags behind that of rigid devices [51]. It is crucial to develop flexible substrates and electrodes with high transparency and mechanical stability [49, 52]. The optoelectronic performance and mechanical stability of the device could be enhanced through the development and optimization of flexible substrates exhibiting high transparency and low Young's modulus, along with electrodes featuring high conductivity and superior flexibility [53].

2.1. Flexible substrates

The selection of a flexible substrate plays an important role in the optoelectronic and mechanical properties of f-PeLEDs. Therefore, f-PeLEDs require substrates with excellent flexibility, high transmittance, and good stability. Transparent polymers such as polyethylene terephthalate (PET), polyethylene naphthalate (PEN), polyimide (PI), and poly(dimethylsiloxane) (PDMS) have the advantages of good flexibility, strong transparency, and light weight and are widely used in flexible devices [48, 54–56]. In addition, emerging substrates such as paper-based materials have also been developed and applied to f-PeLEDs.

2.1.1. Polymer substrates

As shown in Table 1, instead of glass substrates, other flexible substrates have been used to improve the flexibility of PeLEDs [48, 54–56]. For flexible substrates, key parameters such as the glass transition temperature (Tg), thermal expansion coefficient, surface energy, transmittance, and Young's modulus need to be considered [57]. Since the device fabrication process requires high-temperature annealing, a higher Tg indicates better thermal stability [58]. Furthermore, it is crucial to ensure that the coefficient of thermal expansion of the flexible substrate closely matches those of both the HTL and the perovskite layer to avoid internal stress, which could cause the substrate to crack and deteriorate the mechanical properties of the device [57]. Additionally, surface energy could affect the wettability of the solution on the flexible substrate. The lower the surface energy, the worse the wettability of the perovskite solution on the substrate [59]. As a result, the prepared film is uneven and affects the performance of the device. Transmittance and Young's modulus also affect the performance of the device [60]. The higher the transmittance, the higher the color purity of the device [18]. And a higher Young's modulus corresponds to reduced flexibility of the device and a lower tolerance for repeated bending [33].

Table 1
Summary of f-PeLEDs substrates

Substrate	Transition temperature (°C)	CTE (μm/°C)	Surface energy (mJ/m2)	Transmittance	Young modulus Mpa	Ref.
PEN	120	20	40	88%	(3–5) ×103	[57]
PET	90	33	41	90%	(2.8–3) ×103	[57]
PDMS	−125	310	23	85%	3	[58]
PI	270	30	30	85%	(2–3) ×103	[61]

Currently, transparent polymer substrates, such as PET and PEN, are the most commonly used alternatives to glass substrates, with the advantages of low cost and solvent resistance. Among them, PEN contains naphthalene rings in its molecular chains, which provide superior mechanical flexibility and stability as well as a higher transition temperature compared to PET, whose chains contain a benzene ring [47, 62]. However, PEN and PET have poor thermal stability and are incompatible with the high annealing temperatures required during device fabrication [57, 63]. PET is generally limited to disposable sensor applications, whereas PEN, with its superior mechanical strength, is more appropriate for flexible sensor applications [57]. Due to the fact that the Tg of PDMS is one of the lowest among these polymers, it possesses excellent thermal stability and outstanding biocompatibility. Additionally, its low Young's modulus enables it to endure large tensile stress. Therefore, PDMS substrates are utilized in stretchable electronic devices for electronic skin applications [58, 64]. However, due to its large expansion coefficient that makes it difficult to match well with the perovskite layer, as well as its low surface energy, it requires additional treatments such as plasma treatment to improve surface wettability, which limits its application in flexible devices [65]. Moreover, PI refers to a class of polymers that contain an imine ring in their main chain, endowing them with excellent chemical stability, superior dielectric properties, good elasticity, high flexibility, and high transition temperature [57]. However, PI substrates have not been widely applied due to challenges in preparation, such as insolubility or poor solubility, relatively low mechanical strength, and high manufacturing costs [61]. Therefore, considering both the advantages and limitations of flexible substrates along with their production costs, the commonly used substrates are still PEN and PET [33, 66]. Achieving a balanced combination of optical transparency and mechanical flexibility requires strategic structural design and process optimization. At the same time, by considering the influence of other parameters of the substrates on the devices, flexible substrates more suitable for flexible devices could be developed and optimized [61].

2.1.2. Other flexible substrates

Although PET and PEN are widely used, the high roughness, low wettability, and poor low-temperature resistance of flexible substrates may lead to a reduction in device efficiency during the transfer from rigid to flexible substrates [67].

As shown in Figure 3, new materials are chosen as substrates. Norland optical adhesive 63 (NOA63) and Parylene/SU-8 have also been employed as materials for flexible substrates (Figure 3(a) [68]). NOA63 has drawn significant attention owing to its excellent durability, high transparency, and superior processability. Compared with PET and PEN, NOA63 demonstrates greater suitability for high-temperature processes and mechanical deformation, particularly under conditions where the bending radius is less than 1.2 mm [49, 68]. For Parylene, its core functions are ultrathin flexible substrates and encapsulation protection, addressing the mechanical deformation and environmental sensitivity issues of flexible devices. Meanwhile, SU-8 is mainly used for microstructure

Figure 3

(a) Based on NOA63; (b) Parylene substrates of f-PeLEDs structures; (c) schematic of preparing paper-based f-PeLEDs

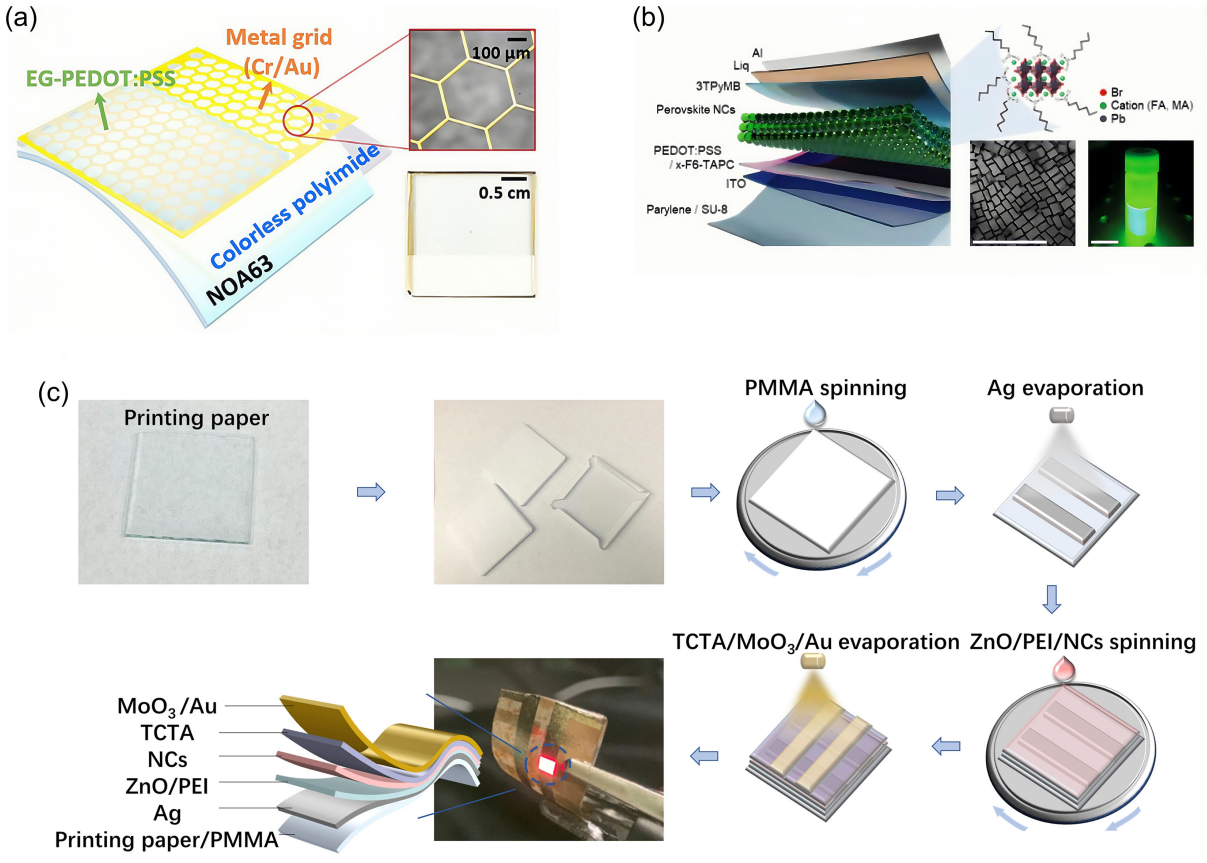

processing and local rigid support (Figure 3(b) [69]). The combination of Parylene and SU-8 can optimize the mechanical reliability, functional integration, and environmental stability of flexible substrates [69]. Flexible polymer substrates will experience deformation and an increase in resistance when exposed to temperatures above the Tg. Although these substrates have excellent flexibility, the poor thermal stability of Parylene and NOA63 substrates (Tg < 150°C) may lead to device degradation or even failure [70]. Moreover, due to the complex fabrication process of these substrates, it is necessary to find new substrates to address these issues [71].

The use of paper-based materials as flexible substrates has been proposed due to their remarkable advantages, including flexibility, biocompatibility, environmental friendliness, renewability, and low cost. Moreover, compared with PET and PEN, the characteristic of paper that can withstand a high temperature of 250°C is more suitable for the annealing process of devices [45]. However, the high roughness of paper usually leads to device damage. To reduce the surface roughness of the paper and further improve the performance of the devices, poly(methyl methacrylate) (PMMA) is used as a coating to reduce surface roughness and effectively prevent solvent penetration during the spin-coating process. Based on this strategy, the f-PeLEDs achieved a peak EQE of 14.3% (Figure 3(c) [45]). Notably, after being bent 1000 times at a small bending radius of 1.5 mm, the brightness degradation was limited to only 29% [67].

2.2. Flexible electrode

2.2.1. ITO electrode

ITO etched on flexible substrates is commonly used as flexible electrodes. As shown in Table 2, devices based on such flexible electrodes have been successfully applied for green, blue, and red light. Notably, the EQE of devices based on this flexible electrode can reach up to 22.1% [33]. However, In and Sn can be released from ITO and diffuse into the upper layer, causing quenching at the interface between the HTL and the perovskite layer, forming defect states, which reduces the hole injection efficiency of the perovskite layer and thus leads to the decline of the luminescence efficiency of f-PeLEDs [72, 73]. In addition, due to the inherent brittleness of ITO electrodes, their stress tolerance is limited.

Table 2
Device structure and properties summary of f-PeLEDs

Device structure	EQE (%)	Lmax (cd/m^2)	Flexibility stability	T50 (min)	Color	Ref.
PET/ITO/PVK/Perovskite+PVAC/ TPBi/LiF/Al	22.1	32000	82% after 2000 cycles with 5 mm radius	52	Green	[33]
PEN/ITO/PEDOT:PSS/Perovskite/ BCP/LiF/Al	–	676	–	–	Green	[74]
ITO/PEN/tTFB/PVK/Perovskite +TEOS/TFPTMS/ TPBi/LiF/Al	16.2	11353	75% after 1000 cycles	–	Green	[66]
NOA63/Polymer-AgNWs/ Zonyl-treated PEDOT:PSS/ Perovskite/TPBi/LiF/Al	3.98	1060	94% after 100 cycles with 2.5 mm radius	–	Green	[49]
PET/ITO/HATCN/TAPC/Perovskite/ PO-T2T/Liq/Al		17550	–	400	Green	[27]
PET/X-PEDOT:PSS/ PEDOT:PSS/Perovskite/ TPBi/LiF/Al		25972	–	–	Green	[75]
PDMS/CNT/Perovskite+PEO/AgNWs	1.1	200	5 mm radius	–	Green	[43]
PET/AgNWs/PEDOT:PSS/Perovskite +PEG+PEABr/TPBI/LiF/Al	10.1	–	–	–	Green	[76]
PET/Graphene/Buf-HIL/Perovskite/ TPBi/LiF/Al	3.8	13000	with 7.5 mm radius	–	Green	[31]
PDMS/PEDOT:PSS+PEO/Perovskite +PEO/EInGa	0.62	15960	40% strain	–	Green	[54]
Polymer/AgNWs/PEDOT:PSS/PVK: TAPC/Perovskite/TmPyPB/CsF/Al	2.6	1000	stable after 1000 cycles with 4 mm radius	–	Green	[77]
PET/AgNWs/ZnO/PEDOT:PSS/ Perovskite/TPBi/LiF/Al	24.5	–	90% after 1000 cycles with3 mm radius	–	Green	[78]
PEN/AgNWs/AgNPs/MXene/ PEDOT:PSS+KCA/Perovskite/ TPBi/LiF/Al	16.5	50000	90% after 500 cycles with 10 mm radius	62	Green	[48]
Parylene/SU-8/ITO/ PEDOT:PSS/Perovskite/ 3TPyMB/Liq/Al	3.84	320	stable after 1000 cycles with 8 mm radius	–	Green	[69]
PI/ITO/Poly-TPD/PFN-Br /Perovskite+$SrBr_2$/TPBi/LiF/Al	13.9	15194	–	11	Green	[79]
PEN/ITO/PEDOS:PSS/PMMA/ Perovskite+PLA/TPBi/LiF/Al	15.9	–	60% after 10 000 cycles with 3 mm radius	–	Green	[28]

(*Continued*)

Table 2
(*Continued*)

Device structure	EQE (%)	Lmax (cd/m^2)	Flexibility stability	T50 (min)	Color	Ref.
PEN/WAW/PEDOT:PSS/Perovskite +P123/TPBi/LiF/Al	11.9	3390	96.5% after bending 1000 cycles with 4.45 mm radius	–	Green	[50]
PET/PEDOT:PSS-IL/Al4083/ TFB/Perovskite/PMMA/ TPBi/LiF/Al	11.6	25566.8	55% after 5000 cycles with 5 mm radius	14.7	Green	[56]
Ag−Ni/Buf-HIL/Perovskite/ TPBi/LiF/Al	9.67	1378	–	–	Green	[73]
PET/Ni-doped A/ZnO/PEI/Perovskite/ MoOx/Ag	4.14	15577	70% after 1200 bending with 0.25 mm radius	–	Green	[18]
PET/ITO/PEDOT:PSS+PSS-Na/ Perovskite/TPBi/LiF/Al	5.91	3936	–	–	Green	[46]
VHB/PI/AgNWs/PEDOT:PSS/TAPC: PVK/Perovskite/TPBi/CsF/Al		3187	1000 stretch-release cycles of 20% tensile strain	–	Green	[80]
PEN/ITO/LiF/Perovskite/ TPBi/NiO_x/Al	1.37	2012	75% after 100 cycles with 5 mm radius	–	Green	[81]
PEN/ITO/TB(MA)/Perovskite/TPBi/ LiF/Al	8.3	2967	–	–	Sky blue	[47]
PET/PEDOT:PSS/Perovskite/TPBi/ LiF/Al	12.8	8300	85% after 100 cycles with 1mm	–	Sky blue	[82]
PI/AgNWs/PEI/PEDOT:PSS/ Perovskite+MDI-PU /TPBi/LiF/Al,	13.5	–	87% after 2000 cycles	7	Sky blue	[55]
NOA63/Ag/ZnO/PEI/Perovskite/ TCTA/MoO3/Au	12.1	1674	75% after 1000 cycles with3 mm radius	80	Red	[1]
PEN/ITO/PEDOT:PSS/Poly-TPD/ PVP/Perovskite/TPBi/LiF/Al	14.3	–	90% after 1000 cycles with 5 mm radius	155	Red	[83]
PI/ITO/PEDOT:PSS/Perovskite/ POT2T/LiF/Al	1	30	–	180	Red	[84]
Label/Ag/ZnO/PEI/Perovskite/TCTA/ MoO/Au	14.3	3615	71% after 1000 cycles with 1.5 mm radius	51	Red	[67]
CPI/Ag/PEDOT:PSS/Poly-TPD/ Perovskite+TS/TPBi/LiF/Al	16.2	–	93% after 5000 cycles with 3 mm radius	216	Red	[34]
Paper/PMMA/Ag/ZnO/Perovskite/ TCTA/MoO3/Au	8.5	1330	75% after 100 cycles with 3 mm radius	16	Red	[45]
Cu/ITO/PEDOT:PSS/Poly-TPD/ Perovskite /TPBi/LiF/Al	15.3	22			Red	[85]
PEN/ITO/PEDOT:PSS/Poly-TPD/ KI/Perovskite/TPBi/LiF/Al	12.7	576	–	40	Deep red	[26]
PI/AgNWs/PEDOT:PSS/polyTPD/ Perovskite+FPMAI/TPBi/LiF/Al	13		no degradation after 10000 cycles with 2 mm radius	–	Near-Infrared	[51]

2.2.2. Graphene electrode

Owing to its high transparency, excellent conductivity, low cost, and superior chemical stability, graphene is considered a promising candidate material for flexible electrodes (Figure 4(a) [31]). Replacing ITO with this chemically inert graphene electrode free of any metal impurities can achieve flexible electrodes that do not quench excitons in f-PeLEDs. Moreover, graphene electrodes exhibit remarkable durability, capable of withstanding over 1000 bending cycles and high bending strains (5.3%) [31].

2.2.3. Metal electrode

Due to the work function of silver nanowires being lower than that of ITO, the scattering of silver nanowires (AgNWs) enhances the coupling of light emission, and their conductivity-transmittance performance is comparable to that of ITO [86]. Furthermore, AgNWs electrodes on flexible substrates demonstrate excellent mechanical robustness under bending conditions [80]. Consequently, as shown in Figure 4(b) [80], AgNWs are considered a promising alternative to ITO as flexible electrodes, with devices based on AgNWs achieving the EQE of 13%, and no performance degradation after being bent 10,000 cycles with a radius of 2 mm [48, 51]. However, the surface of AgNWs is relatively rough and may react with perovskite materials through redox reactions, resulting in generating defect states in perovskite materials, which limit the electroluminescence efficiency of f-PeLEDs [73]. Therefore, through the co-deposition of Ni and Ag (Figure 4(c) [18]), Ag thin film electrodes with low optical loss and thermal stability are obtained. These electrodes exhibited an average visible light transmittance of 80% and a sheet resistance of less than 20 Ω/sq [18]. In addition, Ni can be electroplated onto AgNWs, where Ni covers both the surface and nanogaps of the AgNWs (Figure 4(d) [73]). This not only enhances their conductivity and work function but also facilitates more efficient hole injection into the perovskite layer. Importantly, the Ni shell on AgNWs effectively suppresses the redox reaction between Ag and FAPbBr3, thereby preventing the degradation of the perovskite layer as well as the formation of defect states [73]. After the addition of ZnO, the surface of AgNWs becomes smooth, which prevents direct contact

Figure 4
(a) Device structure of f-PeLED with graphene electrode; (b) SEM images and current efficiency of AgNWs/ITO and AgNWs/PI substrates; (c) schematic representation of the fabrication procedure of doped Ag-based flexible transparent conductors; (d) schematic illustration of the process of Ni electroplating on AgNWs surface; (e) device structure of the f-PeLED on pattern AgNWs/PET substrate

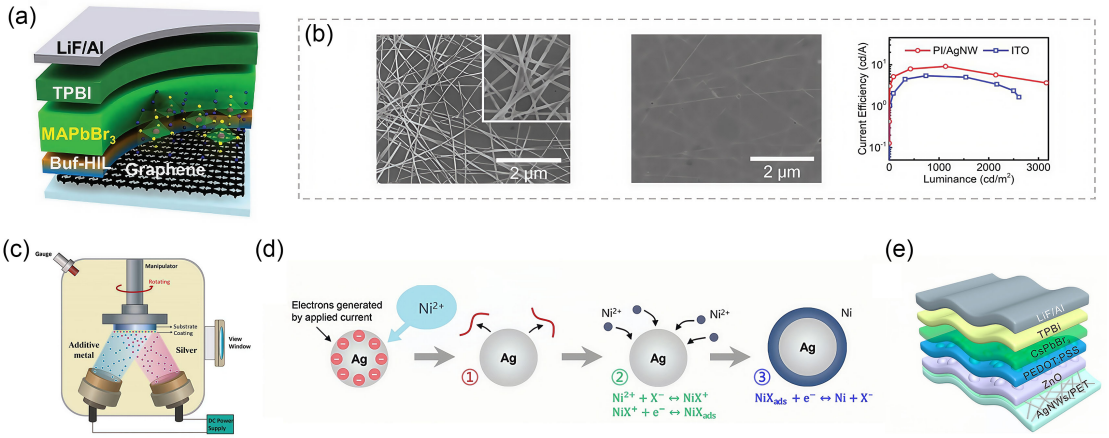

between AgNWs and the perovskite layer, thereby improving the chemical stability of AgNWs. In addition, by integrating AgNWs electrodes with quasi-random nanopatterns on a flexible substrate, the outcoupling efficiency of trapped light is significantly enhanced (Figure 4(e) [78]). As a result, the EQE of green-emitting $CsPbBr_3$ perovskite devices reaches up to 24.5% [78].

2.2.4. Polymer electrode

Poly(3,4-ethylenedioxythiophene): polystyrene sulfonate (PEDOT:PSS) is a conductive polymer with excellent flexibility. However, its conductivity has yet to reach the level required to replace ITO. To enable the application of PEDOT:PSS in flexible electrodes, several strategies have been investigated.

As shown in Figure 5(a) [56], the modification of PEDOT:PSS by adding ionic liquid 1-ethyl-3-methylimidazolium tricyanomethanide (EMIM TCB IL) results in a highly flexible, conductive, and stable transparent electrode. The incorporation of IL facilitates the rearrangement of ions within the PEDOT:PSS film, enhancing its conductivity while increasing the work function of the PEDOT:PSS layer. Furthermore, the IL-modified PEDOT:PSS demonstrates excellent flexibility, retaining 85% of its initial performance after 5000 bending cycles, with an EQE reaching up to 11.6% [56].

In addition, introducing hexa-2,4-diyne-1,6-diol into PEDOT:PSS solution enables the formation of cross-linked PEDOT:PSS films with photo-patterning capabilities. Moreover, it can react with PSS chains and form a cross-linked PEDOT:PSS network, endowing PEDOT:PSS electrodes with photo-patterning capabilities, weakening the electrostatic attraction between PEDOT and PSS chains, and thereby enhancing the conductivity of PEDOT:PSS electrodes [75] (Figure 5(b) [75]).

2.2.5. Composite electrode

Replacing ITO electrodes with alternative materials has become a key strategy. Although the use of graphene, silver nanowires, and organic polymers has enhanced electrode flexibility, challenges such as insufficient device stability, complex preparation process, and poor adhesion still need to be solved [87, 88]. Therefore, the concept of a composite electrode is introduced. The dielectric/metal/dielectric (DMD) electrode exhibits advantages such as diverse structural compositions, adjustable performance, and resistance to bending. Moreover, the optical and electrical properties of the DMD electrode can be adjusted by selecting appropriate materials for the dielectric and metal layers [89, 90]. As shown in Figure 5(c) [50], the WO_3/Au/WO_3 (WAW) electrode is used in f-PeLEDs. WAW exhibits a higher work function (−5.2 eV), which matches well with the energy level of PEDOT:PSS (−5.1 eV), facilitating hole injection and thereby improving the charge injection efficiency of the device. Additionally, due to its superior bending resistance, the WAW electrode enables flexible devices to retain 96.5% of their original current efficiency (CE) after 1000 folding cycles at a bending radius of 4.45 mm [50].

Novel two-dimensional transition metal carbides/nitrides (MXenes) have attracted significant attention due to their high electrical conductivity, excellent thermal dissipation properties, and superior mechanical stability [91, 92]. However, MXenes exhibit issues such as high contact resistance, rough film surfaces, and limited flexibility, which limit device performance [86, 93]. To address these challenges, a composite electrode consisting of 0D silver nanoparticles (AgNPs), 1D AgNWs, 2D MXene, and 3D PEDOT:PSS is developed. This composite electrode integrates the advantages of low-dimensional materials, metals, inorganic semiconductors, and organic semiconductors, resulting in enhanced electrical conductivity, flexibility, smooth surface, and excellent light transmittance. As shown in Figure 5(d) [48], the fabricated f-PeLEDs achieve an EQE of 16.5% and a high luminance of approximately 50,000 cd/m^2 [48].

3. Optimization of Hole Transport Layer

For f-PeLEDs, HTLs located between the perovskite layer and transparent electrode play an important role in the performance and stability of the device [56]. The ideal HTL should possess multiple desirable characteristics, including efficient charge injection, excellent mechanical strength, and high optical transparency [47]. By developing and optimizing HTL materials, effective energy level matching could be achieved, which enhances carrier transport efficiency [78]. Simultaneously, these HTLs could prevent the transport of opposite carriers, further improving device performance [94].

Figure 5
(a) Schematic illustration of the rearrangement of ions in the PEDOT:PSS film before and after the addition of the IL; (b) EQE−V curves (inset: device configuration) of f-PeLED based on patterned X-PEDOT:PSS electrode; (c) structure of f-PeLED based on WAW electrode; (d) J-EQE−V curves and structure of f-PeLED based on composite electrode

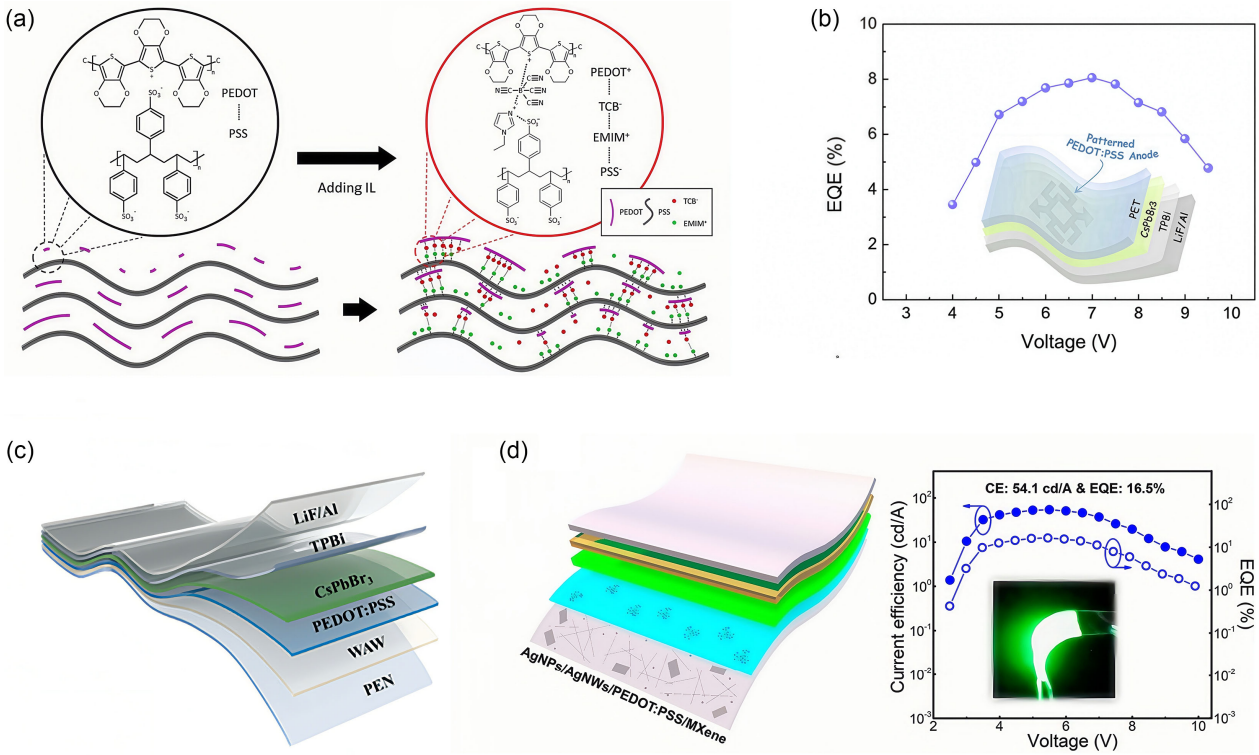

Therefore, various HTLs, such as PEDOT:PSS, poly(9-vinylcarbazole) (PVK), and Nickel oxide (NiO_x), have been developed for application in devices [95, 96]. However, their applications in f-PeLEDs are limited by certain drawbacks, such as the high-temperature annealing and the light-quenching caused by the high trap density of oxygen results [97]. In this section, we review the strategies of improving PEDOT:PSS layer and other suitable HTLs for f-PeLEDs.

3.1. PEDOT:PSS layer

PEDOT:PSS is used not only as an electrode but also employed as an HTL in f-PeLEDs, owing to its superior solution processability and remarkable electrical conductivity [48]. Unfortunately, the inherent acidity and hygroscopic nature of PEDOT:PSS may lead to the corrosion of the underlying electrode, thereby affecting the stability of the device. Additionally, the self-doping effect of PSS^- ions results in the formation of an intermixed region at the interface, which deteriorates the performance of the device [47, 98]. Enhancing the conductivity of PEDOT:PSS through additives and adjusting the energy level alignment through interface engineering are common methods for improving the performance of PEDOT:PSS-based devices.

3.1.1. Instruments

The highest occupied molar orbital (HOMO) energy level of PEDOT:PSS is −5.04 eV, which has a hole injection barrier relative to the valence band of the perovskite at −5.8 eV [49]. The energy level mismatch within the device results in a substantial hole injection barrier, which disrupts the balanced injection of carriers and ultimately deteriorates device performance [99]. The hole injection barrier refers to the significant difference between the highest occupied molecular orbital of the HTL and the valence band of the perovskite layer, forming an energetic barrier [100]. Due to the large hole injection barrier, holes need to overcome an energy barrier to inject into the perovskite light-emitting layer, leading to a reduction in the number of holes entering the perovskite layer [101, 102]. As shown in Figure 6(a), by adding Zonyl FS-300 (Zonyl), isopropanol, poly (sodium 4-styrenesulfonate) (PSS-Na), perfluorinated ionomer, and other additives to the PEDOT:PSS, the potential barrier between HTL and perovskite layer could be reduced, thereby enhancing the hole injection into the perovskite layer and reducing the exciton quenching at the interface [46, 49, 73, 103, 104]. As a result, devices fabricated with the modified HTLs have a significant improvement in both maximum luminance and EQE compared to those using pristine PEDOT:PSS HTLs [46] (Figure 6(b) [49]).

As shown in Figure 6(c) [68], in addition, doping ethylene glycol (EG) into PEDOT:PSS induces a reorganization of the molecular structure in PEDOT:PSS layer, leading to a significant enhancement in the conductivity of HTL by approximately three orders of magnitude (Figure 6(c)) [68]. Amino-functionalized ethanolamine (ETA) could also effectively modify PEDOT:PSS. Upon the incorporation of ETA, the wetting property of the perovskite precursor solution on the HTL is significantly improved. The presence of the hydroxyl group (−OH) in ETA may have promoted the electron-withdrawing inductive effect, which in turn diminishes the electron-donating capability of the amino group and weakens its hydrogen-bonding ability. This process facilitates perovskite films with fewer defects and enhanced luminescence on the ETA-modified PEDOT:PSS substrate, and

Figure 6

(a) The HOMO level of PEDOT:PSS layers with different additives; (b) EQE statistics of device with different additives and side-view images of Zonyl-modified PEDOT:PSS-based f-PeLEDs with different bending radii (insert); (c) schematic illustration of the f-PeLEDs using EG-PEDOT:PSS; (d) histograms of the peak EQEs of f-PeLEDs with flat and patterned structures on the PEDOT:PSS substrate with ETA additive; (e) photos of f-PeLEDs under a 4 V bias before (top) and after (bottom) stretching to 40% strain; (f) elongation at break of the soft polymer/PEDOT:PSS:PSS blends prepared from their aqueous solutions without additive or with added DMSO or EG

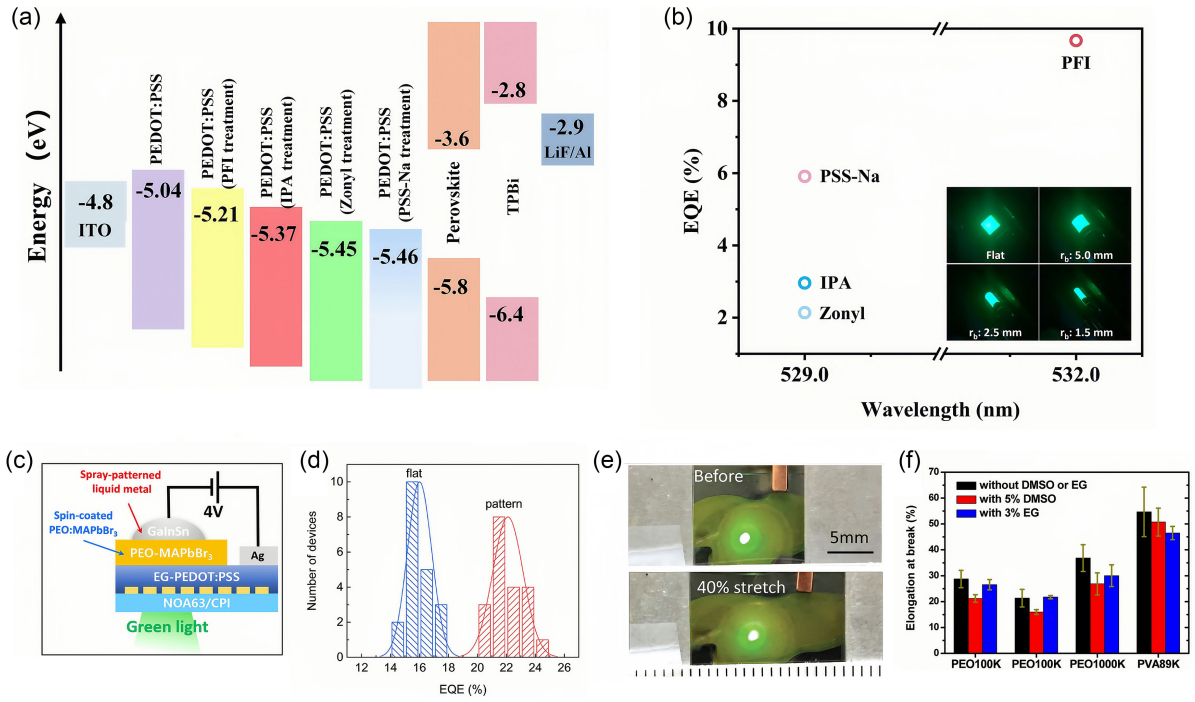

trap-mediated non-radiative recombination losses can be minimized to the greatest extent [78] (Figure 6(d) [78]). Additionally, introducing sulfuric acid (H_2SO_4)-treated PEDOT:PSS into (AgNWs) enables the formation of ordered crystalline PEDOT:PSS nanofibers, which reduces the surface roughness and resistance of the flexible electrode while enhancing the electrical conductivity of PEDOT:PSS [49].

Since the failure strain of PEDOT:PSS/polymer composites is higher than that of pristine PEDOT:PSS, poly(ethylene oxide) (PEO) is added to PEDOT:PSS and directly spin-coated onto PDMS to be used as a transparent electrode and HTL (Figure 6(e) [54]). On this basis, the f-PeLEDs have good mechanical robustness and can be reversibly stretched up to 40% strain for 100 cycles without affecting device performance [54]. Additionally, PEDOT:PSS can also be modified with polyvinyl alcohol (PVA) to enhance its elongation at break from 2% to 55% and its conductivity from 0.2 to 75 S cm-1. Furthermore, adding dimethyl sulfoxide (DMSO) into the polymer-blended solution could further elevate the conductivity to 172 S cm-1, thereby optimizing the performance of PEDOT:PSS in f-PeLEDs applications [105] (Figure 6(f) [105]).

3.1.2. Interface engineering

The use of HTLs with deeper HOMO energy levels, such as PVK [106, 107] and poly(4-butylphenyl-diphenyl-amine) (polyTPD) [34, 51, 85], deposited on PEDOT:PSS to form a gradient energy level for hole injection (Figure 7(a) [83]). This structure, which resembles a multi-layer HTL, effectively enhances hole injection capability and improves energy level matching, thereby demonstrating significant improvement effects [108–110].

A PVP intermediate layer can also be spin-coated on top of PEDOT:PSS /Poly-TPD to enhance the wettability of the substrate [83]. As shown in Figure 7(b) [77], by combining the deep HOMO energy level of PVK and the high hole mobility of 4,4'-cyclohexylidenebis[N,N-bis(4-methylphenyl)benzenamine] (TAPC) [111], a composite layer consisting of PVK and TAPC is introduced to further enhance the performance of the PEDOT:PSS HTL, thereby improving the hole transport mobility for balanced charge carriers in the device [77].

Potassium iodide (KI) is a typical dipolar molecule with superior thermal conductivity compared to other inorganic ligands. By inserting an additional KI passivation layer between the PEDOT:PSS/Poly-TPD and the perovskite layer, the optical properties of the perovskite film can be significantly enhanced, leading to improvements in film uniformity, compactness, and thermal stability (Figure 7(c) [26]). Furthermore, the KI layer facilitates increased carrier mobility, enabling balanced charge injection in f-PeLEDs and reducing Auger recombination and Joule heating [26].

As shown in Figure 7(d), due to the significant difference in charge mobility between the HTL and TPBi (ETL), a thin insulating PMMA layer is inserted between the perovskite layer and HTL to enable charge injection into the perovskite through tunneling [28]. The reduced energy barrier between PVK and the perovskite layer facilitates efficient hole injection, enabling PVK to be a suitable material for application in f-PeLEDs [33]. Moreover, due to the hydrophobicity of PVK, it could protect the perovskite from the limitations of atmospheric moisture and interfacial exciton quenching [112]. Spin-coating poly(ether imide) (PEI) on the transparent electrode could enhance the wettability of PEDOT:PSS on the underlying layer [55]. As shown in Table 2, we summarize the device structures of f-PeLEDs for green, blue, and red light, as

Figure 7
(a) Schematic of the energy diagram with Poly-TPD; (b) schematic of the energy diagram with TAPC; (c) EQE−V curves and structure of f-PeLED with KI; (d) schematic of the energy diagram with PMMA; (e) schematic diagram of the device configuration of p-i-n planar f-PeLEDs (insert: the molecular structure of PEDOT:PSS and TB(MA) and the images of quasi-2D perovskite film under UV lamp excitation)

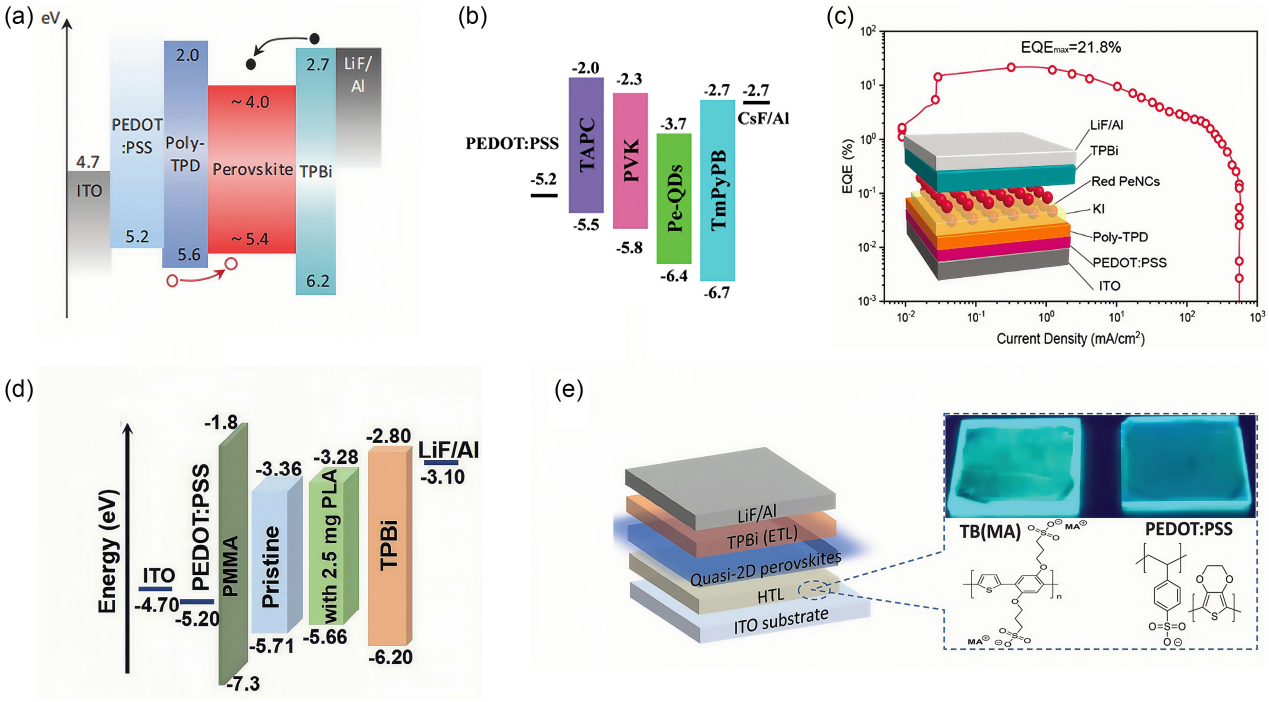

well as their corresponding optoelectronic performance, mechanical properties, and stability.

3.2. Other hole transport layers

For f-PeLEDs, apart from employing PEDOT:PSS as the HTL, their performance can be further improved by selecting alternative materials for the HTLs. A new water-soluble conjugated polyelectrolyte with CH3NH3+(MA^+) counterion, termed as TB(MA), is used as the HTL to replace PEDOT:PSS in device fabrication. Its intrinsic hydrophilicity facilitates the growth of high-quality quasi-2D perovskite films with a dense and uniform morphology. Moreover, the MA^+ counterions in TB(MA) effectively passivate the interface defects at the perovskite/HTL interface [47] (Figure 7(e) [47]). NiO_x, vanadium oxide (VO_x), tungsten oxide (WO_x), and other oxide materials are used as HTLs in rigid PeLEDs due to their superior material stability, high carrier mobility, and enhanced interface adhesion with perovskite layers [46, 113, 114]. These materials are also expected to be extended to the field of f-PeLEDs, providing potential solutions for improving their performance.

4. Improvement of Perovskite Layer

The EQE and mechanical stability of f-PeLEDs are significantly constrained by the intrinsic defects in perovskite films. For instance, the defects and poor surface morphology caused by the more difficult control of the surface properties of perovskite films on flexible substrates lead to poor optical and electrical performance, as well as the inherent mechanical brittleness of polycrystalline perovskites. Therefore, it is highly desirable to develop effective methods to optimize the perovskite quality and flexible performance in f-PeLEDs.

In lead-based perovskites, a significant number of internal defects are the cause of non-radiative recombination of carriers [115]. The internal defects are mainly point defects, which are caused by dangling bonds and incorrect bonding of ionic bonds that lead to structural damage [116]. The EQE and mechanical stability of f-PeLEDs are significantly constrained by the intrinsic defects in perovskite films [117]. For instance, the defects and poor surface morphology caused by the more difficult control of the surface properties of perovskite films on flexible substrates lead to poor optical and electrical performance, as well as the inherent mechanical brittleness of polycrystalline perovskites. Defect passivation could effectively prevent the generation of uncoordinated ions and dangling bonds caused by halogen migration, thereby improving the quality of perovskite layers, enhancing the luminous efficiency of devices, and prolonging their lifespan [118]. Therefore, it is highly desirable to develop effective methods to optimize the perovskite quality and flexible performance in f-PeLEDs. In this section, we will discuss the latest progress in optimizing perovskite films using additive engineering and composition engineering.

4.1. Additive engineering

4.1.1. Lewis base additive

For Pb-based perovskites, the uncoordinated Pb^{2+} caused by halide ion segregation at the perovskite surface or interface is a primary factor limiting device performance. To address this issue, organic small-molecule Lewis bases containing lone-pair electron functional groups, such as carbonyl group (C=O), phosphorus oxide

Figure 8

(a) Schematic illustration of the interaction between perovskite and PI, structure of PI and PTM; (b) chemical structure of TS ligands, the optimized configuration structure and E_{ads} of the ligands interacting with PNCs based on density functional theory (DFT) calculation; (c) fracture energy and PLQY of perovskite films without or with various additives; (d) schematic illustration of formed silica network (left: TEOS; right: TFPTMS) and the interaction with perovskite; (e) structure of MPI-PU

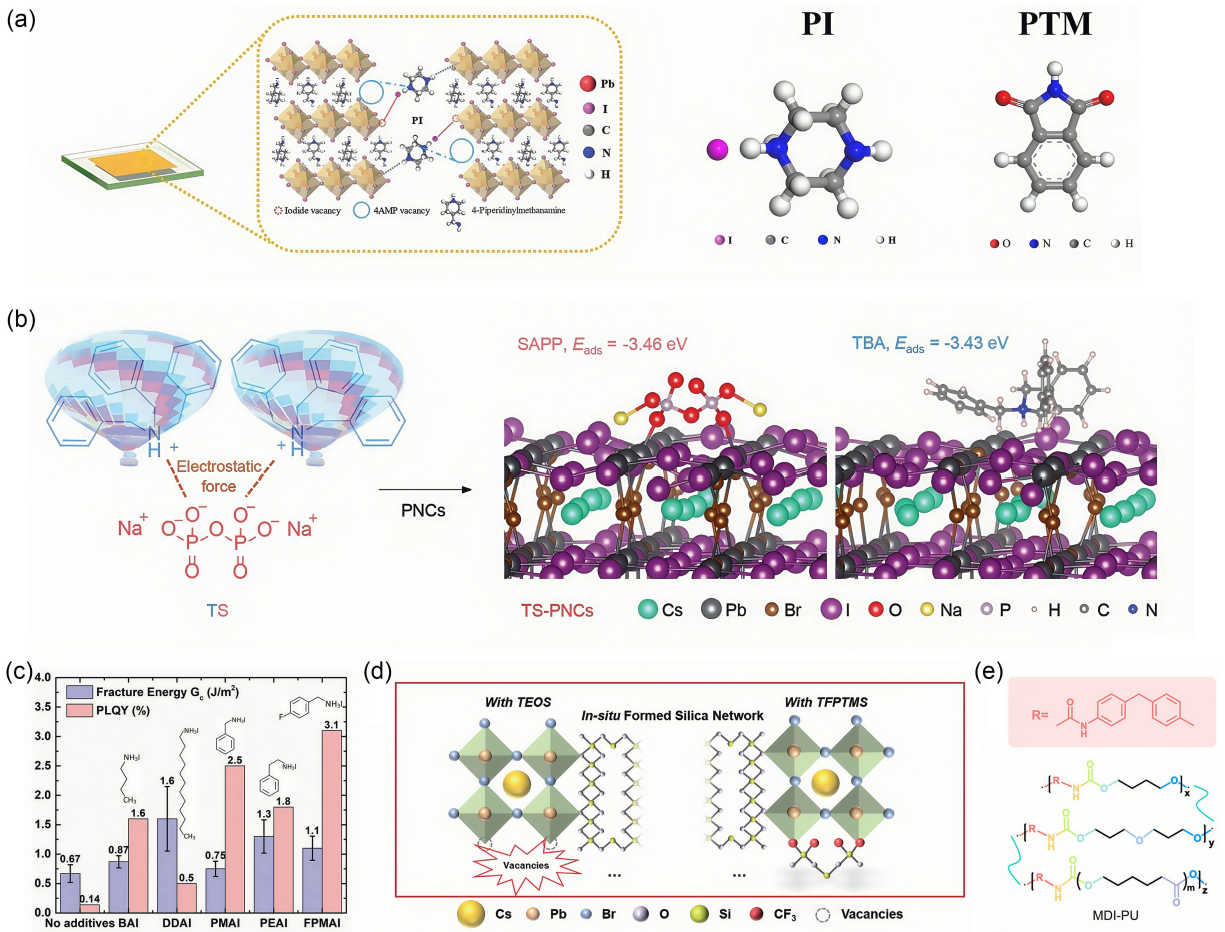

(P=O) and its derivatives, hydroxyl (−OH), and carboxyl (−COOH), have been developed as additives [119–122]. These molecules can effectively coordinate with uncoordinated lead ions (Lewis acids), compensating their charge and achieving defect passivation, which ultimately enhances device stability and efficiency [123].

As shown in Figure 8(a) [124], organic small-molecule additives such as piperazine iodide (PI) and phthalimide (PTM) not only enhance the crystallinity of perovskite films but also effectively passivate defects by altering the local electron density, thereby suppressing non-radiative charge recombination and improving the photovoltaic performance and stability of the devices [124].

Conventional Lewis bases, such as sodium acid pyrophosphate (SAPP), exhibit poor solubility in non-polar perovskite nanocrystals (PNCs) dispersion due to their high degree of ionization and the significant negative charge density of multi-dentate anions, thus restricting their utility in PNCs. Tribenzyl organic cation (tribenzylamine, TBA) is utilized as a carrier and reacts with SAPP via high-temperature proton exchange to form TBA-SAPP (TS). The multibranched non-polar aromatic rings of TBA enable the TS to dissolve in toluene (Figure 8(b) [34]). Furthermore, both TBA and SAPP can effectively interact with PNCs, enhancing interfacial adhesion between the PNCs and adjacent layers while simultaneously passivating exposed Pb^{2+} defects. This dual functionality additive addresses mechanical instability and significantly improves the performance of f-PLEDs. Specifically, these devices demonstrate robustness over 5000 folding cycles with a small radius of 1 mm and achieve a high EQE of 16.2% in the pure-red range [34].

4.1.2. Organic molecular additives

Due to the fact that organic components can form coulombic interactions or hydrogen bonds with perovskites, larger organic ammonium halides are used as additives to enhance the flexibility and improve the photoelectric and mechanical properties of the resulting perovskite films. As shown in Figure 8(c) [51], for instance, butylammonium iodide, dodecylammonium iodide, benzylammonium iodide, phenethylammonium iodide, and 4-fluorobenzylammonium iodide (FPMAI), these five additives have different alkyl chain lengths, molecular sizes, and dipole moments. During the stretching process, molecules with longer alkyl chains can maintain stronger intermolecular interactions at a greater stretching distance before complete separation, while molecules with shorter alkyl chains will be completely separated after a shorter stretching distance. Therefore, the longer the alkyl chain length, the stronger the interactions, leading to larger energy

dissipation during the cohesive fracture process and consequently enhancing the mechanical properties [125]. However, as the length of the alkyl chain increases, the ability of the additive to achieve complete surface coverage diminishes. Therefore, additives with shorter alkyl chains are more likely to achieve better surface coverage, passivate traps, and improve photoelectric properties [51]. These organic-containing additives are indeed beneficial for constructing flexible perovskite films, but they also sacrifice the charge transport capability and affect the photoelectric performance of the devices. To simultaneously enhance mechanical properties and photoelectric characteristics, it is one way to introduce molecules with self-healing ability as additives, such as fluorinated (3,3,3-trifluoropropyl) trimethoxysilane (TFPTMS) and FPMAI, as well as diphenylmethane diisocyanate polyurethane (MDI-PU), etc. (Figure 8(d) [66] and (e) [55]).

After adding TFPTMS to the perovskite precursor solution, the abundant Si-O-Si groups can coordinate with the uncoordinated lead ions through Lewis acid-base interaction. In addition, the alkyl fluoride chains give the perovskite film with self-healing ability, and the rich hydrogen bonds between silanol groups and halogen ions make the perovskite film excellent flexible without sacrificing photovoltaic performance. Ultimately, a highly efficient f-PeLED with an EQE of 16.2% is achieved [66]. Devices incorporating the fluorine-containing additive FPMAI demonstrate markedly improved performance and achieve a peak EQE of up to 13% [51].

As an additive, MDI-PU can connect brittle perovskite crystals via carbamate bonds to enhance the flexibility and bendability of perovskite films. Additionally, it can chelate non-coordinated Pb^{2+} of the perovskite films and effectively passivate defects at grain boundaries. The harmful cracks generated during repeated deformation can be efficiently self-repaired through the intramolecular/intermolecular hydrogen-bonding networks of MDI-PU under repeated deformation. After 2000 cycles of bending and twisting operations, the initial efficiencies are retained at 87.8% and 80.7%, respectively [55].

4.1.3. Polymer additives

Polymers can form cross-linked networks with perovskites to enhance the mechanical toughness of the films. Additionally, the functional groups at the polymer terminals can effectively passivate defects and eliminate pinholes on the film surface, leading to improved optical and electrical properties of the films.

Ethyl cellulose (EC) is applied in $CsPbI_3$ nanocrystals (NCs). EC is a long-chain polymer composed of six-membered heterocyclic units containing hydroxyl and ethoxy groups, exhibiting excellent flexibility. The hydrophobic ether groups in EC significantly enhance the environmental stability of the NCs. Moreover, the cross-linking interactions between EC and perovskite NCs improved the mechanical robustness of the perovskite layer, enabling stable photoluminescence even after repeated bending (Figure 9(a) [1]). Consequently, f-PeLED based on EC-passivated $CsPbI_3$ NCs achieves an EQE of 12.1% and demonstrates minimal brightness decay after 1000 bending cycles at a radius of 3 mm [1].

Introducing highly flexible polylactic acid (PLA) polymer into quasi-2D perovskite films and forming a polymer cross-linking network can also enhance the mechanical stability of the films. In addition, the C=O functional groups in PLA (Figure 9(b) [28]) can coordinate with the unsaturated Pb^{2+} sites, leading to effective passivation of defects within the perovskite film [28].

The incorporation of polymer polyethylene oxide-polypropylene oxide-polyethylene oxide triblock copolymer (P123) into perovskite not only accelerates the crystallization process but also promotes the formation of uniform and small-sized perovskite grains. Furthermore, as shown in Figure 9(c) [50], the OH- and C-O functional groups in P123 can effectively anchor the crystal structure of perovskite and passivate unsaturated Pb^{2+}. As a result, after being folded 1000 times at a bending radius of 4.45 mm, the CE of the flexible devices retains 96.5% of its initial value [50].

As shown in Figure 9(d) [33], the polyvinyl acetate (PVAC) with C=O and C-O-C functional groups can effectively passivate Pb^{2+} defects, suppress the formation of pinholes on the film surface, and enhance both the optical and electrical properties of the perovskite film. Due to the hydrophobic nature of PVAC and its capability to form a polymer network, the Young's modulus of the perovskite film is significantly reduced, thereby improving the mechanical bending stability. After 2000 bending cycles at a radius of 5 mm, the mechanical stability of retaining 82% of its initial performance, providing a robust foundation for the development of high-performance flexible optoelectronic devices [33]. Although the optoelectronic performance of the device is enhanced after the addition of PVAC, the EQE of the device is still slightly behind that of the device based on a nanopatterned flexible substrate. In future research, the two optimization strategies could be combined to simultaneously passivate defects and suppress the light loss of the substrate, which would further improve the device performance.

The hydrophilicity of PEO enables the perovskite precursor solution to diffuse smoothly, which helps increase the nucleation density of perovskite, reduce the grain size, and fill the gaps between grains to obtain a stretchable and smooth surface film [126]. Even under a 40% linear strain, these devices can still emit uniform green light [54]. PEO can also protect the perovskite film from the influence of humidity changes and increase the stability of the device [32]. It can also enhance the uniformity of perovskite films, improve their surface coverage, and effectively reduce the density of grain boundary defects. Furthermore, the two-dimensional passivation strategy is integrated to further enhance device performance. It is found that PEABr enables the formation of mixed-dimensional $CsPbBr_3$ perovskites, which exhibit reduced grain size. The synergistic combination of PEO and PEABr additives makes morphology control of perovskite films, leading to optimized film quality [52, 76, 78].

4.2. Composition engineering

The surface morphology and grain size distribution of perovskite films are critical factors influencing the performance of f-PeLEDs. To obtain a smooth and uniform perovskite layer, magnificent efforts have focused on enlarging grain size, eliminating pinholes, and minimizing cracks [124]. In addition to the various additives described above, the film quality can also be further optimized by adjusting the concentration of the precursor solution and incorporating metal cations.

Dendritic CsSnI3 films are fabricated by simply controlling the precursor concentration. As shown in Figure 9(e) [127], this design not only enhances electron injection but also restricts the non-directional diffusion of holes. Moreover, it demonstrates significant advantages in flexible devices, showing almost no morphological change after 2000 bending cycles. The fabricated f-PeLEDs can still maintain 93.4% of the initial EQE after 50 bending cycles [127].

A strategy for modulating the phase distribution of quasi-2D perovskite films using divalent strontium cation (Sr^{2+}) is proposed. It is found that strontium bromide ($SrBr_2$) can effectively regulate the growth of quasi-2D perovskites by appropriately enhancing their formation energy, thereby fully eliminating the low-n phases (Figure 9(f) [79]). The EQE of the quasi-2D green f-PeLED fabricated based on this film achieves a peak EQE of 13.9% [79].

Figure 9

(a) Energy level arrangement of each layer in the device structure with adding EC in perovskite; (b) schematic illustrations of cross-linked perovskite/PLA polymer; (c) schematic of perovskite modification; (d) structure of PVAC and EQE distribution of devices with different organic materials treatment; (e) schematic illustration of the charge carriers transport and recombination process in the f-PeLEDs based on flat and dendritic $CsSnI_3$ film; (f) schematic diagram of the impacts of $PbBr_2$ and $SrBr_2$ on the growth of quasi-2D perovskites

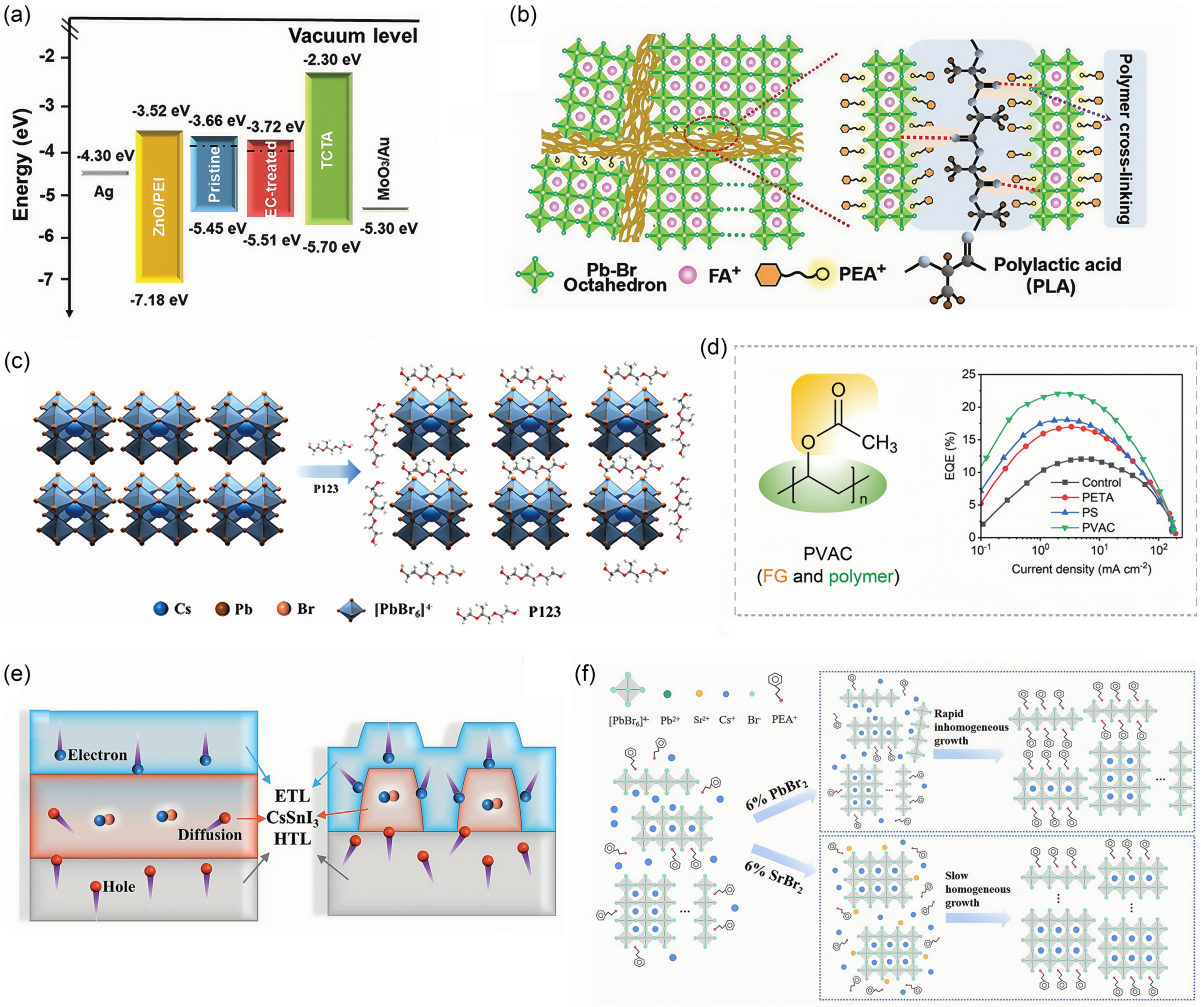

5. Novel Fabrication Method of f-PeLED Devices

The commonly used method for preparing perovskite layers is to spin-coat the perovskite precursor solution onto the substrate and then directly perform thermal annealing to evaporate the residual solvent and promote crystallization [32]. Unlike the traditional spin-coating method for preparing inverted p-i-n type f-PeLEDs, there are now many new fabrication methods. In this section, we will discuss new fabrication methods including spin coating, vacuum evaporation, blade coating, and inkjet printing.

5.1. Spin coating

The one-step spin-coating method is the earliest technique applied to the preparation of perovskite thin films. This method is convenient to operate and has a low cost. Moreover, the primary procedure involves uniformly depositing the perovskite precursor solution onto the substrate, followed by crystallization of the perovskite through spin-coating and annealing processes. But after spin-coating the perovskite precursor solution, the resulting perovskite layer exhibits high surface roughness and large grain size.

As shown in Figure 10(a) [74], flash light annealing technology can rapidly heat the perovskite film to 320°C using intense near-infrared light from the flash lamp. This process promotes the rapid formation of a dense recrystallized structure, reduces grain size, enhances radiative recombination, suppresses leakage current, and avoids radiative damage to the material [74]. Because perovskite is sensitive to conditions such as water and oxygen, f-PeLEDs would degrade when exposed to the environment. The application of encapsulation techniques could effectively isolate the devices from these harmful elements, thereby significantly enhancing their stability [128]. For example, by using the encapsulation growth method, scotch tape is closely shielded on the top of the perovskite film during annealing (Figure 10(b) [82]). This approach not only encapsulates the film but also retains the residual DMSO solution for an extended period, thereby providing sufficient growth time to obtain high-quality perovskite films with uniform morphology, dense structure, and low defect density.

Figure 10

(a) Schematic illustrations of the flash-induced ultrafast recrystallization of perovskite; (b) schematic diagrams for the encapsulation growth method of quasi-2D perovskite films; (c) schematic diagram of the $CsPbBr_3$ layer thermal vacuum co-evaporation deposition process in conjunction with in situ dynamic thermal crystallization; (d) schematic showing the fabrication of printed f-PeLED and the disadvantage of blade coating

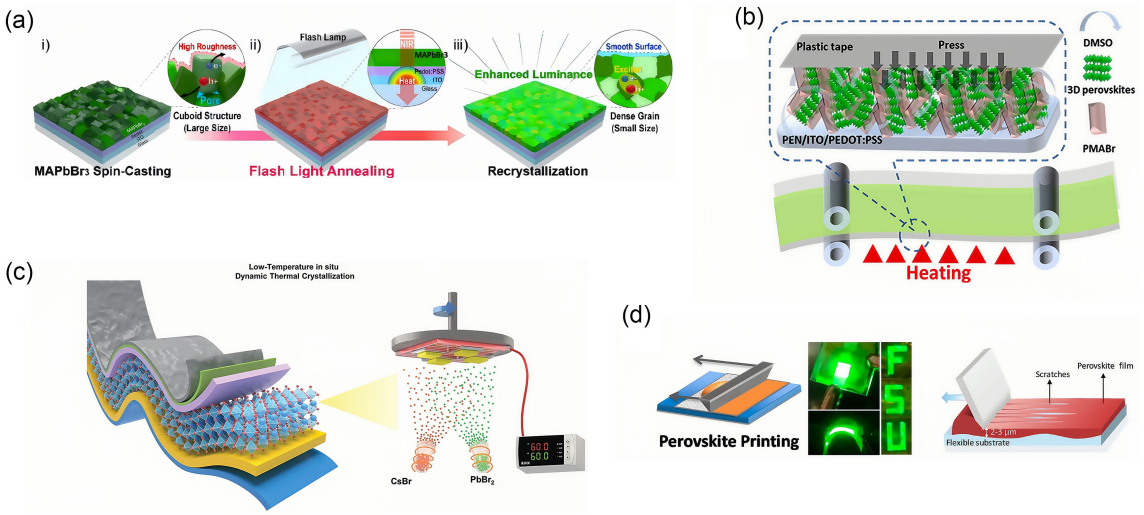

Efficient sky-blue f-PeLEDs are successfully fabricated, achieving the EQE of up to 12.8% [82]. However, the spin-coating method cannot guarantee the uniformity of large-area perovskite films, which limits the demand for large-scale commercial development.

5.2. Vacuum-based deposition

The rapid evaporation of the solvent during solution processing may produce the formation of non-uniform films, while the poor solubility of CsBr in organic solvents seriously restricts the practical application of LEDs [27]. For vacuum-based deposition (VBD), there is no solubility limit, making it suitable for depositing all inorganic perovskites (Figure 10(c) [27]), and it can also form protective coatings on rough substrates [81]. VBD primarily enhances device performance by optimizing the composition and annealing temperature of perovskites and the thickness of functional layers. Additionally, it can combine VBD with continuous thermal annealing to promote in situ dynamic thermal crystallization, thereby effectively regulating the crystal size and density of perovskites [27, 81]. However, VBD is associated with relatively high costs, and incorporating various passivation materials into the film remains challenging.

5.3. Blade coating

Alternative techniques such as the blade coating and inkjet printing have been introduced for the fabrication of f-PeLEDs [83]. As shown in Figure 10(d) [43, 83], the blade coating method involves depositing perovskite solution onto a carbon nanotubes (CNTs)/polymer, uniformly spreading the solution using a blade, and annealing it in air. The pattern of the metal electrodes can be defined via a Kapton mask, enabling the fabrication of devices with various sizes and patterns. These devices can be stretched to a curvature radius of 5 mm [43]. However, when fabricating tens-of-nanometers-thick films for f-PeLEDs, the working depth of the blade coater is about several micrometers. This relatively narrow depth inevitably results in noticeable scratches on the film surface, which are more clear on large-area flexible substrates [83].

5.4. Inkjet printing

As shown in Figure 11(a) [84], inkjet printing is a noncontact technology, with the distance between the print head and the substrate typically ranging from millimeters to centimeters. This feature enables the method to be more tolerant of variations in the surface height of flexible substrates, and it allows for the deposition of both lead-based and lead-free perovskites [83, 84]. However, inkjet printing requires specially formulated printable ink, precisely tuned substrate wettability, and suppression of the coffee ring effect, among other requirements [32, 83]. Therefore, novel strategies have been developed to enhance the inkjet printing process. For example, liquid self-encapsulation inkjet printing involves directly depositing perovskite ink onto a liquid PDMS precursor, thereby forming in situ a self-encapsulated perovskite single-crystal-embedded PDMS structure (Figure 11(c) [129]). The spatial confinement effect of the liquid PDMS significantly slows down the perovskite crystallization process and promotes the directional growth of single crystals, obtaining perovskite single crystals with excellent environmental stability and flexibility [129].

Furthermore, as shown in Figure 11(b) [32], all-inkjet-printed f-PeLEDs are proposed, introducing a simplified device structure, all-solution-based and all-printing process, simultaneous annealing method, and programmed automatic trajectory control. The rheological behavior, viscosity, wettability, and uniformity of each ink are studied and optimized to achieve optimal printing outcomes on flexible substrates. The f-PeLEDs are printed on PDMS/PET substrates through this technology, exhibiting excellent flexibility, being able to be repeatedly bent to a curvature radius of 2.5 mm for thousands of times without showing any obvious performance

Figure 11
(a) Schematic illustrations of the inkjet printing of perovskite; (b) schematic diagrams illustrating the fabrication processes of the all-inkjet-printed f-PeLEDs; (c) schematic illustration of inkjet printing of the perovskite single-crystal array-embedded PDMS film; (d) photos and photoluminescence images of large-area (6×9 cm^2) perovskite films on PEN/ITO substrates with different components; (e) schematic illustration of a multicolor skin-attachable f-PeLED

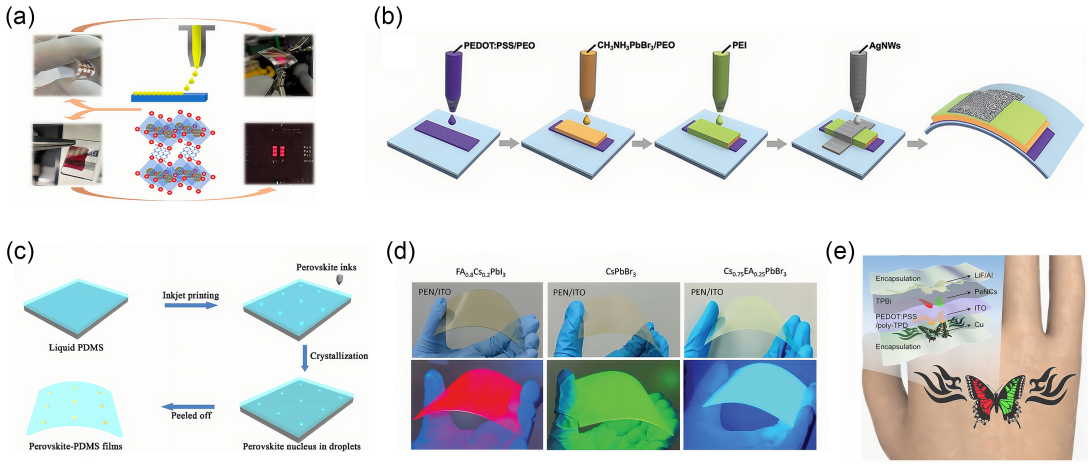

degradation. Moreover, the manufacturing process could be completed within only 25 minutes [32].

To address the challenge of substrate wettability adjustment in inkjet printing, a double-hole transport layer and a wetting interfacial layer are utilized to improve surface wettability. In addition, by manipulating the fluidic and evaporation dynamics of the perovskite wet layer through solvent engineering, the coffee ring effect can be suppressed, resulting in uniform perovskite films on flexible substrates (Figure 11(d) [83]). When integrated into devices, the resulting f-PeLEDs achieve a maximum EQE of 14.3% [83].

However, the use of additives for achieving uniform inkjet printing, as well as the challenge of forming ultrathin pixels, has restricted the widespread adoption of inkjet printing. The development of double-layer transfer printing process for perovskite nanocrystal (PeNCs) film and organic charge transport layers (Figure 11(e) [85]) is a printing process that enables the fabrication of monochrome patterns in RGB pixel patterns of 2550 pixels per inch, successfully preventing internal cracking of the perovskite nanocrystal during the transfer printing process [85].

6. Conclusion and Outlook

Since the initial report on f-PeLEDs, researchers have systematically enhanced flexible substrates with high-temperature resistance and mechanical stability, as well as electrodes exhibiting superior conductivity and flexibility. Additionally, the HTLs have been improved to achieve better compatibility with the perovskite layer, while the perovskite film has been optimized to further improve the mechanical robustness and optoelectronic performance. Moreover, an increasing number of novel preparation techniques have been developed for the fabrication of f-PeLEDs. Therefore, the f-PeLEDs fabricated based on these advancements have enabled applications in ultrathin skin-attachable displays and wearable electronics.

In this review, we have summarized the strategies employed in recent years to enhance the flexibility and optoelectronic performance of devices. Based on the above advancements, it could be concluded that f-PeLEDs hold great potential as next-generation high-performance optoelectronic devices. Nevertheless, several critical challenges remain to be addressed.

As mentioned above, various flexible substrates based on transparent polymers have been explored. However, due to their high surface roughness, poor transmittance, and poor thermal stability, it is necessary to develop flexible substrates that integrate high transparency, better flexibility, excellent mechanical stability, and cost-effectiveness. In addition, diverse flexible electrodes such as graphene electrodes, metal electrodes, polymer electrodes, two-dimensional material electrodes, and composite electrodes have been developed. In terms of the existing reports, composite electrodes have been utilized through the combination of materials with different photoelectric properties and functions to overcome the shortcomings of single electrodes. Therefore, future research could take advantage of the characteristics of composite electrodes, integrate the advantages of multiple electrodes, and develop flexible electrodes with high conductivity, better flexibility, and excellent mechanical properties.

For the HTLs, the conductivity and flexibility can be enhanced by adding additives, the energy barrier can be modulated through interface engineering, and the energy level alignment is optimized to improve the wettability of the perovskite film on the HTLs, thereby enhancing the quality of the perovskite film. In addition, we expect to develop new HTL materials such as metal oxides, self-assembled molecules, and organic polymers.

The perovskite layer plays a crucial role in f-PeLEDs. Lewis acids, organic molecules and polymers as additives could effectively passivate defects and enhance mechanical stability, flexibility and photoelectric properties of defects could be effectively passivated, the mechanical robustness of perovskite films. Furthermore, adjusting the concentration of the precursor solution and modifying the composition of the perovskite could improve the quality of the perovskite films. Therefore, we expect that subsequent studies can introduce more additives with synergistic functions to further achieve efficient and stable f-PeLEDs.

Although the spin-coating method has been optimized and alternative techniques such as blade coating and vacuum deposition have been developed, issues such as poor coverage and complex preparation processes still need to be addressed. In addition, most of these methods are suited for small-area devices. Therefore, further exploration is required to develop processing

techniques suitable for large-area f-PeLEDs by combining inkjet printing and other process methods. In future research, the flexibility of other functional layers in the device and the adhesion between layers could also be improved by developing new materials and interface engineering, which is of great significance for the commercialization of flexible devices.

As most flexible substrates are plastic substrates, the process from production to disposal of plastic substrates would cause many environmental problems, such as the release of toxic chemicals, soil pollution, and the difficulty of degradation. To solve this issue, in addition to recyclable substrates like paper substrates, people should develop more recyclable and biodegradable flexible substrates to replace flexible polymer substrates, in order to reduce environmental pollution.

For f-PeLEDs, the necessary condition for their conversion to practical applications is that the prepared f-PeLEDs do not affect their optoelectronic and mechanical properties after repeated stretching, bending, and folding. Future research still needs to focus on flexible substrates, flexible electrodes, HTLs, and perovskite layers. Lead-based f-PeLEDs have made rapid progress, but the toxicity of lead has hindered their further commercial application. To address this issue, future research should develop lead-free perovskites, integrating the excellent photoelectric properties of lead-based perovskites with their non-toxicity. For instance, tin-based f-PeLEDs and the application of double perovskite structures could be further optimized. These methods could promote f-PeLEDs application in wearable technology, intelligent electronics, and other fields.

To achieve the commercial production of f-PeLEDs, it is necessary to consider the production of large-area f-PeLEDs. As the preparation area increases, the defects in perovskite films will also be further expanded. Furthermore, conventional spin-coating methods are not suitable for preparing large-area f-PeLEDs. Therefore, more novel preparation methods should be explored, for example, roll-to-roll fabrication processes to reduce manufacturing costs, as well as improving inkjet printing technology to fabricate large-area and high-resolution patterns.

Funding Support

This work is sponsored by the National Natural Science Foundation of China (No. 22175049) and the Open Fund of Guangdong Provincial Key Laboratory of Luminescence from Molecular Aggregates, Guangzhou 510640, China (South China University of Technology) (2024-kllma-03).

Conflicts of Interest

The authors declare that they have no conflicts of interest to this work.

Data Availability Statement

Data sharing is not applicable to this article as no new data were created or analyzed in this study.

Author Contribution Statement

Qi Han: Methodology, Validation, Investigation, Data curation, Writing – original draft, Writing – review & editing, Visualization. **Peng Han:** Formal analysis, Resources. **Daizhe Wang:** Software. **Yong Zhang:** Conceptualization, Supervision, Project administration, Funding acquisition.

References

[1] Sun, S., Jia, P., Lu, M., Lu, P., Gao, Y., Zhong, Y., . . . , & Bai, X. (2022). Enhanced flexibility and stability of emissive layer enable high-performance flexible light-emitting diodes by cross-linking of biomass material. *Advanced Functional Materials*, *32*(33), 2204286. https://doi.org/10.1002/adfm.202204286

[2] Liu, X., Xu, W., Bai, S., Jin, Y., Wang, J., Friend, R. H., & Gao, F. (2021). Metal halide perovskites for light-emitting diodes. *Nature Materials*, *20*(1), 10–21. https://doi.org/10.1038/s41563-020-0784-7

[3] Xue, Q., Sun, J., Huang, Y., Zhu, M., Pei, Z., Li, H., . . . , & Zhi, C. (2017). Recent progress on flexible and wearable supercapacitors. *Small*, *13*(45), 1701827. http://doi.org/10.1002/smll.201701827

[4] Bao, Z., & Chen, X. (2016). Flexible and stretchable devices. *Advanced Materials*, *28*(22), 4177–4179. http://doi.org/10.1002/adma.201601422

[5] Abbas, A., Luo, Y., Ahmad, W., Mustaqeem, M., Kong, L., Chen, J., . . . , & Liang, Q. (2024). Recent progress, challenges, and opportunities in 2D materials for flexible displays. *Nano Today*, *56*, 102256. https://doi.org/10.1016/j.nantod.2024.102256

[6] Han, T.-H., Lee, Y., Choi, M.-R., Woo, S.-H., Bae, S.-H., Hong, B. H., . . . , & Lee, T.-W. (2012). Extremely efficient flexible organic light-emitting diodes with modified graphene anode. *Nature Photonics*, *6*(2), 105–110. https://doi.org/10.1038/nphoton.2011.318

[7] Choi, M. K., Yang, J., Kang, K., Kim, D. C., Choi, C., Park, C., . . . , & Kim, D.-H. (2015). Wearable red–green–blue quantum dot light-emitting diode array using high-resolution intaglio transfer printing. *Nature Communications*, *6*(1), 7149. https://doi.org/10.1038/ncomms8149

[8] Kim, Y. H., Cho, H., Heo, J.-H., Kim, T.-S., Myoung, N., Lee, C.-L., . . . , & Lee, T. W. (2015). Multicolored organic/inorganic hybrid perovskite light-emitting diodes. *Advanced Materials*, *27*(7), 1248–1254. https://doi.org/10.1002/adma.201403751

[9] Yokota, T., Nakamura, T., Kato, H., Mochizuki, M., Tada, M., Uchida, M., . . . , & Someya, T. (2020). A conformable imager for biometric authentication and vital sign measurement. *Nature Electronics*, *3*(2), 113–121. https://doi.org/10.1038/s41928-019-0354-7

[10] van Breemen, A. J. J. M., Ollearo, R., Shanmugam, S., Peeters, B., Peters, L. C. J. M., van de Ketterij, R. L., . . . , & Gelinck, G. H. (2021). A thin and flexible scanner for fingerprints and documents based on metal halide perovskites. *Nature Electronics*, *4*(11), 818–826. https://doi.org/10.1038/s41928-021-00662-1

[11] Yamagishi, K., Kirino, I., Takahashi, I., Amano, H., Takeoka, S., Morimoto, Y., & Fujie, T. (2019). Tissue-adhesive wirelessly powered optoelectronic device for metronomic photodynamic cancer therapy. *Nature Biomedical Engineering*, *3*(1), 27–36. https://doi.org/10.1038/s41551-018-0261-7

[12] Choi, M. K., Yang, J., Hyeon, T., & Kim, D.-H. (2018). Flexible quantum dot light-emitting diodes for next-generation displays. *npj Flexible Electronics*, *2*(1), 10. http://doi.org/10.1038/s41528-018-0023-3

[13] Yoo, J. J., Seo, G., Chua, M. R., Park, T. G., Lu, Y., Rotermund, F., . . . , & Seo, J. (2021). Efficient perovskite

solar cells via improved carrier management. *Nature*, *590*(7847), 587–593. https://doi.org/10.1038/s41586-021-03285-w

[14] Cho, H., Jeong, S.-H., Park, M.-H., Kim, Y.-H., Wolf, C., Lee, C.-L., . . . , & Lee, T.-W. (2015). Overcoming the electroluminescence efficiency limitations of perovskite light-emitting diodes. *Science*, *350*(6265), 1222–1225. https://doi.org/10.1126/science.aad1818

[15] Liu, Z., Qiu, W., Peng, X., Sun, G., Liu, X., Liu, D., . . . , & Su, S. (2021). Perovskite light-emitting diodes with EQE exceeding 28% through a synergetic dual-additive strategy for defect passivation and nanostructure regulation. *Advanced Materials*, *33*(43), 2103268. https://doi.org/10.1002/adma.202103268

[16] Yu, R., Li, C., Zhao, B., & Tan, Z. (2024). Frontiers in green perovskite light-emitting diodes. *Laser & Photonics Reviews*, *18*(4), 2300780. http://doi.org/https://doi.org/10.1002/lpor.202300780

[17] Zhang, L., Mei, L., Wang, K., Lv, Y., Zhang, S., Lian, Y., . . . , & Ding, L. (2023). Advances in the application of perovskite materials. *Nano-Micro Letters*, *15*(1), 177. https://doi.org/10.1007/s40820-023-01140-3

[18] Zhang, C., Huang, Q., Cui, Q., Ji, C., Zhang, Z., Chen, X., . . . , & Guo, L. J. (2019). High-performance large-scale flexible optoelectronics using ultrathin silver films with tunable properties. *ACS Applied Materials & Interfaces*, *11*(30), 27216–27225. https://doi.org/10.1021/acsami.9b08289

[19] Xu, W., Hu, Q., Bai, S., Bao, C., Miao, Y., Yuan, Z., . . . , & Gao, F. (2019). Rational molecular passivation for high-performance perovskite light-emitting diodes. *Nature Photonics*, *13*(6), 418–424. https://doi.org/10.1038/s41566-019-0390-x

[20] Yu, Y., Wang, B., Shen, Y., Su, Z., Zhang, K., Ren, H., . . . , & Li, Y. (2024). Regulating perovskite crystallization through interfacial engineering using a zwitterionic additive potassium sulfamate for efficient pure-blue light-emitting diodes. *Angewandte Chemie International Edition*, *63*(7), e202319730. https://doi.org/10.1002/anie.202319730

[21] Herz, L. M. (2017). Charge-carrier mobilities in metal halide perovskites: Fundamental mechanisms and limits. *ACS Energy Letters*, *2*(7), 1539–1548. https://doi.org/10.1021/acsenergylett.7b00276

[22] Sun, C., Jiang, Y., Cui, M., Qiao, L., Wei, J., Huang, Y., . . . , & Yuan, M. (2021). High-performance large-area quasi-2D perovskite light-emitting diodes. *Nature Communications*, *12*(1), 2207. https://doi.org/10.1038/s41467-021-22529-x

[23] Tan, Z.-K., Saberi Moghaddam, R., Lai, M. L., Docampo, P., Higler, R., Deschler, F., . . . , & Friend, R. H. (2014). Bright light-emitting diodes based on organometal halide perovskite. *Nature Nanotechnology*, *9*(9), 687–692. https://doi.org/10.1038/nnano.2014.149

[24] Fakharuddin, A., Gangishetty, M. K., Abdi-Jalebi, M., Chin, S.-H., bin Mohd Yusoff, A. R., Congreve, D. N., . . . , & Bolink, H. J. (2022). Perovskite light-emitting diodes. *Nature Electronics*, *5*(4), 203–216. http://doi.org/10.1038/s41928-022-00745-7

[25] Li, X.-Z., Ye, Y., Cao, Y., Zhang, D., Lin, Y., Chang, J., . . . , & Wang, J. (2025). Tin-halide perovskites for light-emitting diodes. *Chemical Society Reviews, 54*(14), 6697–6725. https://doi.org/10.1039/D5CS00340G

[26] Chen, C., Xuan, T., Yang, Y., Huang, F., Zhou, T., Wang, L., & Xie, R.-J. (2022). Passivation layer of potassium iodide yielding high efficiency and stable deep red perovskite light-emitting diodes. *ACS Applied Materials & Interfaces*, *14*(14), 16404–16412. https://doi.org/10.1021/acsami.2c00621

[27] Chen, C., Han, T.-H., Tan, S., Xue, J., Zhao, Y., Liu, Y., . . . , & Yang, Y. (2020). Efficient flexible inorganic perovskite light-emitting diodes fabricated with $CsPbBr_3$ emitters prepared via low-temperature in situ dynamic thermal crystallization. *Nano Letters*, *20*(6), 4673–4680. https://doi.org/10.1021/acs.nanolett.0c01550

[28] Li, T., Gao, Y., Wu, Y., Lu, M., Hu, J., Zhang, Y., . . . , & Yan, F. (2024). Polymer cross-linking strategy enables high performance and high mechanical stability flexible quasi-2D perovskite light-emitting diodes. *Advanced Optical Materials*, *12*(10), 2302053. https://doi.org/10.1002/adom.202302053

[29] Feng, S.-C., Shen, Y., Hu, X.-M., Su, Z.-H., Zhang, K., Wang, B.-F., . . . , & Li, Y.-Q. (2024). Efficient and stable red perovskite light-emitting diodes via thermodynamic crystallization control. *Advanced Materials*, *36*(44), 2410255. http://doi.org/10.1002/adma.202410255

[30] Xing, Z., Jin, G., Du, Q., Pang, P., Liu, T., Shen, Y., . . . , & Ma, D. (2024). Ions-induced assembly of perovskite nanocomposites for highly efficient light-emitting diodes with EQE exceeding 30%. *Advanced Materials*, *36*(46), 2406706. https://doi.org/10.1002/adma.202406706

[31] Seo, H.-K., Kim, H., Lee, J., Park, M.-H., Jeong, S.-H., Kim, Y.-H., . . . , & Lee, T.-W. (2017). Efficient flexible organic/inorganic hybrid perovskite light-emitting diodes based on graphene anode. *Advanced Materials*, *29*(12), 1605587. http://doi.org/10.1002/adma.201605587

[32] Zhao, J., Lo, L.-W., Wan, H., Mao, P., Yu, Z., & Wang, C. (2021). High-speed fabrication of all-inkjet-printed organometallic halide perovskite light-emitting diodes on elastic substrates. *Advanced Materials*, *33*(48), 2102095. http://doi.org/10.1002/adma.202102095

[33] Liu, C., Zhang, D., Sun, J., Li, D., Xiong, Q., Lyu, B., . . . , & Choy, W. C. H. (2024). Constructing multi-functional polymeric-termination surface enables high-performance flexible perovskite LEDs. *Advanced Functional Materials*, *34*(45), 2404791. https://doi.org/10.1002/adfm.202404791

[34] Lyu, B., Li, D., Ke, C., Liang, H., Sun, J., Xiong, Q., . . . , & Choy, W. C. H. (2025). Tribenzyl organic cations carried multidentate X-type Lewis soft base for high-performance foldable perovskite light-emitting diodes. *Advanced Materials*, *37*(25), 2415211. https://doi.org/10.1002/adma.202415211

[35] Kumar, S., Jagielski, J., Kallikounis, N., Kim, Y.-H., Wolf, C., Jenny, F., . . . , & Shih, C.-J. (2017). Ultrapure green light-emitting diodes using two-dimensional formamidinium perovskites: Achieving recommendation 2020 color coordinates. *Nano Letters*, *17*(9), 5277–5284. https://doi.org/10.1021/acs.nanolett.7b01544

[36] Hassan, Y., Park, J. H., Crawford, M. L., Sadhanala, A., Lee, J., Sadighian, J. C., . . . , & Snaith, H. J. (2021). Ligand-engineered bandgap stability in mixed-halide perovskite LEDs. *Nature*, *591*(7848), 72–77. http://doi.org/10.1038/s41586-021-03217-8

[37] Liu, Y., Cui, J., Du, K., Tian, H., He, Z., Zhou, Q., . . . , & Jin, Y. (2019). Efficient blue light-emitting diodes based on quantum-confined bromide perovskite nanostructures. *Nature Photonics*, *13*(11), 760–764. https://doi.org/10.1038/s41566-019-0505-4

[38] Cao, Y. B., Zhang, D., Zhang, Q., Qiu, X., Zhou, Y., Poddar, S., . . . , & Fan, Z. (2023). High-efficiency, flexible and large-area

red/green/blue all-inorganic metal halide perovskite quantum wires-based light-emitting diodes. *Nature Communications*, *14*(1), 4611. https://doi.org/10.1038/s41467-023-40150-y

[39] Zhao, X., & Tan, Z.-K. (2020). Large-area near-infrared perovskite light-emitting diodes. *Nature Photonics*, *14*(4), 215–218. https://doi.org/10.1038/s41566-019-0559-3

[40] Dai, X., Zhang, Z., Jin, Y., Niu, Y., Cao, H., Liang, X., . . . , & Peng, X. (2014). Solution-processed, high-performance light-emitting diodes based on quantum dots. *Nature*, *515*(7525), 96–99. http://doi.org/10.1038/nature13829

[41] Stoppa, M., & Chiolerio, A. (2014). Wearable electronics and smart textiles: A critical review. *Sensors*, *14*(7), 11957–11992. https://doi.org/10.3390/s140711957

[42] Wang, J., Han, D., Zhao, B., Zang, Z., Ji, H., Liu, L., & Wang, N. (2025). Push-pull effect enables large-area lead-free Perovskite light-emitting diodes via electron directional transfer. *Laser & Photonics Reviews, 19*(18), e00727. https://doi.org/10.1002/lpor.202500727

[43] Bade, S. G. R., Li, J., Shan, X., Ling, Y., Tian, Y., Dilbeck, T., . . . , & Yu, Z. (2016). Fully printed halide perovskite light-emitting diodes with silver nanowire electrodes. *ACS Nano*, *10*(2), 1795–1801. https://doi.org/10.1021/acsnano.5b07506

[44] Kim, T.-H., Lee, C.-S., Kim, S., Hur, J., Lee, S., Shin, K. W., . . . , & Hwang, S. (2017). Fully stretchable optoelectronic sensors based on colloidal quantum dots for sensing photoplethysmographic signals. *ACS Nano*, *11*(6), 5992–6003. https://doi.org/10.1021/acsnano.7b01894

[45] Qin, F., Lu, M., Sun, S., Lu, P., Feng, N., Gao, Y., . . . , & Zhang, Y. (2023). Paper substrates based flexible red-emitting perovskite nanocrystal light-emitting diodes. *IEEE Electron Device Letters*, *44*(7), 1056–1059. https://doi.org/10.1109/LED.2023.3277852

[46] Kim, H., Ra, H. N., Kim, J. S., Paek, S.-H., Park, J., & Kim, Y. C. (2020). Improved performance of flexible perovskite light-emitting diodes with modified PEDOT:PSS hole transport layer. *Journal of Industrial and Engineering Chemistry*, *90*, 117–121. https://doi.org/10.1016/j.jiec.2020.07.003

[47] Liu, Y., Zhang, L., Chen, S., Liu, C., Li, Y., Wu, J., . . . , & Xu, B. (2021). Water-soluble conjugated polyelectrolyte hole transporting layer for efficient sky-blue perovskite light-emitting diodes. *Small*, *17*(37), 2101477. https://doi.org/10.1002/smll.202101477

[48] Cao, F., You, M., Kong, L., Dou, Y., Wu, Q., Wang, L., . . . , & Yang, X. (2022). Mixed-dimensional mxene-based composite electrodes enable mechanically stable and efficient flexible perovskite light-emitting diodes. *Nano Letters*, *22*(10), 4246–4252. https://doi.org/10.1021/acs.nanolett.2c01517

[49] Lee, S. Y., Nam, Y. S., Yu, J. C., Lee, S., Jung, E. D., Kim, S.-H., . . . , & Song, M. H. (2019). Highly efficient flexible perovskite light-emitting diodes using the modified PEDOT:PSS hole transport layer and polymer–silver nanowire composite electrode. *ACS Applied Materials & Interfaces*, *11*(42), 39274–39282. https://doi.org/10.1021/acsami.9b10771

[50] Sun, K., Bao, Z., Guo, X., Zou, D., Lv, Y., Liang, J., & Liu, X. (2024). Crystallization regulation and defect passivation of high-performance flexible perovskite light-emitting diodes based on novel dielectric/metal/dielectric transparent electrodes. *Advanced Optical Materials*, *12*(5), 2301752. https://doi.org/10.1002/adom.202301752

[51] Zhao, L., Rolston, N., Lee, K. M., Zhao, X., Reyes-Martinez, M. A., Tran, N. L., . . . , & Rand, B. P. (2018). Influence of bulky organo-ammonium halide additive choice on the flexibility and efficiency of perovskite light-emitting devices. *Advanced Functional Materials*, *28*(31), 1802060. https://doi.org/10.1002/adfm.201802060

[52] Payandeh, M., Ahmadi, V., Arabpour Roghabadi, F., Nazari, P., Ansari, F., Brenner, P., . . . , & Abdollahi Nejand, B. (2020). High-brightness perovskite light-emitting diodes using a printable silver microflake contact. *ACS Applied Materials & Interfaces*, *12*(10), 11428–11437. https://doi.org/10.1021/acsami.9b18527

[53] Zheng, W., Lin, R., Zhang, Z., Liao, Q., Liu, J., & Huang, F. (2017). An ultrafast-temporally-responsive flexible photodetector with high sensitivity based on high-crystallinity organic–inorganic perovskite nanoflake. *Nanoscale*, *9*(34), 12718–12726. https://doi.org/10.1039/C7NR04395C

[54] Bade, S. G. R., Shan, X., Tran Hoang, P., Li, J., Geske, T., Cai, L., . . . , & Yu, Z. (2017). Stretchable light-emitting diodes with organometal-halide-perovskite–polymer composite emitters. *Advanced Materials*, *29*(23), 1607053. https://doi.org/10.1002/adma.201607053

[55] Qian, X., Shen, Y., Zhang, L.-J., Guo, M., Cai, X.-Y., Lu, Y., . . . , & Lee, S.-T. (2022). Bio-inspired pangolin design for self-healable flexible perovskite light-emitting diodes. *ACS Nano*, *16*(11), 17973–17981. https://doi.org/10.1021/acsnano.2c06118

[56] Han, J. H., Sadhukhan, P., & Myoung, J.-M. (2023). Highly flexible and stable green perovskite light-emitting diodes based on IL-modified PEDOT:PSS film. *Applied Surface Science*, *641*, 158493. https://doi.org/10.1016/j.apsusc.2023.158493

[57] Aleksandrova, M. (2016). Specifics and challenges to flexible organic light-emitting devices. *Advances in Materials Science and Engineering*, *2016*(1), 4081697. https://doi.org/10.1155/2016/4081697

[58] Wolf, M. P., Salieb-Beugelaar, G. B., & Hunziker, P. (2018). PDMS with designer functionalities—Properties, modifications strategies, and applications. *Progress in Polymer Science*, *83*, 97–134. https://doi.org/10.1016/j.progpolymsci.2018.06.001

[59] Li, Z., Chai, Z., Wang, G., Zhang, J., Wang, T., Zhao, D., . . . , & Lu, X. (2025). High-performance flexible electronics fabricated using a surface energy-directed assembly process on ultrathin polyimide substrates. *Small, 21*(29), 2409458. https://doi.org/10.1002/smll.202409458

[60] Yu, J., Wang, M., & Lin, S. (2016). Probing the soft and nanoductile mechanical nature of single and polycrystalline organic–inorganic hybrid perovskites for flexible functional devices. *ACS Nano*, *10*(12), 11044–11057. https://doi.org/10.1021/acsnano.6b05913

[61] Shi, S., Yao, L., Ma, P., Jiao, Y., Zheng, X., Ning, D., . . . , & Li, W. (2021). Recent progress in the high-temperature-resistant PI substrate with low CTE for CIGS thin-film solar cells. *Materials Today Energy*, *20*, 100640. https://doi.org/10.1016/j.mtener.2021.100640

[62] Du, P., Li, J., Wang, L., Sun, L., Wang, X., Xu, X., . . . , & Tang, J. (2021). Efficient and large-area all vacuum-deposited perovskite light-emitting diodes via spatial confinement. *Nature Communications*, *12*(1), 4751. https://doi.org/10.1038/s41467-021-25093-6

[63] Khan, S., Lorenzelli, L., & Dahiya, R. S. (2015). Technologies for printing sensors and electronics over large flexible

substrates: A review. *IEEE Sensors Journal*, *15*(6), 3164–3185. https://doi.org/10.1109/JSEN.2014.2375203

[64] Qi, D., Zhang, K., Tian, G., Jiang, B., & Huang, Y. (2021). Stretchable electronics based on PDMS substrates. *Advanced Materials*, *33*(6), 2003155. https://doi.org/10.1002/adma.202003155

[65] Yang, X., Huang, W., Dong, H., & Zha, J. (2025). Smart polydimethylsiloxane materials: Versatility for electrical and electronic devices applications. *Advanced Materials*, *37*(17), 2500472. https://doi.org/10.1002/adma.202500472

[66] Zang, J., Cai, L., Zou, Y., Li, Y., Bai, G., Hong, Z., . . . , & Sun, B. (2022). Self-healing perovskite films enabled by fluorinated cross-linked network targeting flexible light-emitting diode. *Advanced Optical Materials*, *10*(16), 2200566. https://doi.org/10.1002/adom.202200566

[67] Qin, F., Li, T., Lu, M., Sun, S., Lu, P., Li, X., . . . , & Bai, X. (2023). Highly efficient and flexible perovskite nanocrystal light-emitting diodes on disposable paper substrates. *ACS Applied Materials & Interfaces*, *15*(40), 47278–47285. https://doi.org/10.1021/acsami.3c10070

[68] Jin, S. W., Lee, Y. H., Yeom, K. M., Yun, J., Park, H., Jeong, Y. R., . . . , & Ha, J. S. (2018). Highly durable and flexible transparent electrode for flexible optoelectronic applications. *ACS Applied Materials & Interfaces*, *10*(36), 30706–30715. https://doi.org/10.1021/acsami.8b10190

[69] Jinno, H., Shivarudraiah, S. B., Asbjörn, R., Vagli, G., Marcato, T., Eickemeyer, F. T., . . . , & Shih, C. (2024). Indoor self-powered perovskite optoelectronics with ultraflexible monochromatic light source. *Advanced Materials*, *36*(5), 2304604. https://doi.org/10.1002/adma.202304604

[70] Zardetto, V., Brown, T. M., Reale, A., & di Carlo, A. (2011). Substrates for flexible electronics: A practical investigation on the electrical, film flexibility, optical, temperature, and solvent resistance properties. *Journal of Polymer Science Part B: Polymer Physics*, *49*(9), 638–648. https://doi.org/10.1002/polb.22227

[71] Lu, M., Wu, H., Zhang, X., Wang, H., Hu, Y., Colvin, V. L., . . . , & Yu, W. W. (2019). Highly flexible $CsPbI_3$ perovskite nanocrystal light-emitting diodes. *ChemNanoMat*, *5*(3), 313–317. https://doi.org/10.1002/cnma.201800359

[72] Kim, S., Oh, H., Jeong, I., Kang, G., & Park, M. (2021). Influence of a solvent trap in ITO/PEN substrates on the performance of flexible perovskite solar cells and light-emitting diodes. *ACS Applied Electronic Materials*, *3*(7), 3207–3217. https://doi.org/10.1021/acsaelm.1c00385

[73] Kang, H., Choi, S.-R., Kim, Y.-H., Kim, J. S., Kim, S., An, B.-S., . . . , & Cho, J. H. (2020). Electroplated silver–nickel core–shell nanowire network electrodes for highly efficient perovskite nanoparticle light-emitting diodes. *ACS Applied Materials & Interfaces*, *12*(35), 39479–39486. https://doi.org/10.1021/acsami.0c10386

[74] Jung, D. H., Park, J. H., Lee, H. E., Byun, J., Im, T. H., Lee, G. Y., . . . , & Kim, S. O. (2019). Flash-induced ultrafast recrystallization of perovskite for flexible light-emitting diodes. *Nano Energy*, *61*, 236–244. https://doi.org/10.1016/j.nanoen.2019.04.061

[75] Liu, L., Yang, H., Zhang, Z., Wang, Y., Piao, J., Dai, Y., . . . , & Chen, S. (2023). Photopatternable and highly conductive PEDOT:PSS electrodes for flexible perovskite light-emitting diodes. *ACS Applied Materials & Interfaces*, *15*(17), 21344–21353. https://doi.org/10.1021/acsami.3c03108

[76] Cheng, L.-P., Huang, J.-S., Shen, Y., Li, G.-P., Liu, X. K., Li, W., . . . , & Tang, J.-X. (2019). Efficient $CsPbBr_3$ perovskite light-emitting diodes enabled by synergetic morphology control. *Advanced Optical Materials*, *7*(4), 1801534. https://doi.org/10.1002/adom.201801534

[77] Zhao, F., Chen, D., Chang, S., Huang, H., Tong, K., Xiao, C., . . . , & Pei, Q. (2017). Highly flexible organometal halide perovskite quantum dot based light-emitting diodes on a silver nanowire–polymer composite electrode. *Journal of Materials Chemistry C*, *5*(3), 531–538. https://doi.org/10.1039/C6TC04934F

[78] Shen, Y., Li, M. N., Li, Y. Q., Xie, F. M., Wu, H. Y., Zhang, G. H., . . . , & Tang, J. X. (2020). Rational interface engineering for efficient flexible perovskite light-emitting diodes. *ACS Nano*, *14*(5), 6107–6116. http://doi.org/10.1021/acsnano.0c01908

[79] Wang, J., Li, D., Wang, J., & Peng, J. (2022). Efficient emission of quasi-two-dimensional perovskite films cast by inkjet printing for pixel-defined matrix light-emitting diodes. *Materials Futures*, *1*(4), 045301. https://doi.org/10.1088/2752-5724/ac9b2d

[80] Li, Y.-F., Chou, S.-Y., Huang, P., Xiao, C., Liu, X., Xie, Y., . . . , & Pei, Q. B. (2019). Stretchable organometal-halide-perovskite quantum-dot light-emitting diodes. *Advanced Materials*, *31*(22), 1807516. https://doi.org/10.1002/adma.201807516

[81] Li, J., Du, P., Li, S., Liu, J., Zhu, M., Tan, Z., . . . , & Tang, J. (2019). High-throughput combinatorial optimizations of perovskite light-emitting diodes based on all-vacuum deposition. *Advanced Functional Materials*, *29*(51), 1903607. https://doi.org/10.1002/adfm.201903607

[82] Liu, Y., Yu, Z., Chen, S., Park, J. H., Jung, E. D., Lee, S., . . . , & Lee, B. R. (2021). Boosting the efficiency of quasi-2D perovskites light-emitting diodes by using encapsulation growth method. *Nano Energy*, *80*, 105511. https://doi.org/10.1016/j.nanoen.2020.105511

[83] Liu, H., Shi, G., Khan, R., Chu, S., Huang, Z., Shi, T., . . . , & Xiao, Z. (2024). Large-area flexible perovskite light-emitting diodes enabled by inkjet printing. *Advanced Materials*, *36*(8), 2309921. https://doi.org/10.1002/adma.202309921

[84] Vescio, G., Sanchez-Diaz, J., Frieiro, J. L., Sánchez, R. S., Hernández, S., Cirera, A., . . . , & Garrido, B. (2022). 2D PEA_2SnI_4 inkjet-printed halide perovskite LEDs on rigid and flexible substrates. *ACS Energy Letters*, *7*(10), 3653–3655. https://doi.org/10.1021/acsenergylett.2c01773

[85] Kwon, J. I., Park, G., Lee, G. H., Jang, J. H., Sung, N. J., Kim, S. Y., . . . , & Choi, M. K. (2022). Ultrahigh-resolution full-color perovskite nanocrystal patterning for ultrathin skin-attachable displays. *Science Advances*, *8*(43), eadd0697. https://doi.org/10.1126/sciadv.add0697

[86] Hu, L., Kim, H. S., Lee, J.-Y., Peumans, P., & Cui, Y. (2010). Scalable coating and properties of transparent, flexible, silver nanowire electrodes. *ACS Nano*, *4*(5), 2955–2963. https://doi.org/10.1021/nn1005232

[87] Lee, Y., Bae, S., Jang, H., Jang, S., Zhu, S.-E., Sim, S. H., . . . , & Ahn, J.-H. (2010). Wafer-scale synthesis and transfer of graphene films. *Nano Letters*, *10*(2), 490–493. https://doi.org/10.1021/nl903272n

[88] Avouris, P., & Dimitrakopoulos, C. (2012). Graphene: Synthesis and applications. *Materials Today*, *15*(3), 86–97. https://doi.org/10.1016/S1369-7021(12)70044-5

[89] Kinner, L., Dimopoulos, T., Ligorio, G., List-Kratochvil, E. J. W., & Hermerschmidt, F. (2021). High performance organic light-emitting diodes employing ITO-free and flexible

TiO_x/Ag/Al:ZnO electrodes. *RSC Advances*, *11*(28), 17324–17331. https://doi.org/10.1039/D1RA02214H

[90] Manekkathodi, A., Chen, B., Kim, J., Baek, S.-W., Scheffel, B., Hou, Y., ..., & Sargent, E. (2019). Solution-processed perovskite-colloidal quantum dot tandem solar cells for photon collection beyond 1000 nm. *Journal of Materials Chemistry A*, *7*(45), 26020–26028. https://doi.org/10.1039/C9TA11462A

[91] Liu, Z., & Alshareef, H. N. (2021). MXenes for optoelectronic devices. *Advanced Electronic Materials*, *7*(9), 2100295. https://doi.org/10.1002/aelm.202100295

[92] Ahn, S., Han, T., Maleski, K., Song, J., Kim, Y., Park, M., ..., & Lee, T. (2020). A 2D titanium carbide MXene flexible electrode for high-efficiency light-emitting diodes. *Advanced Materials*, *32*(23), 2000919. https://doi.org/10.1002/adma.202000919

[93] Gaynor, W., Hofmann, S., Christoforo, M. G., Sachse, C., Mehra, S., Salleo, A., ..., & Leo, K. (2013). Color in the corners: ITO-free white OLEDs with angular color stability. *Advanced Materials*, *25*(29), 4006–4013. https://doi.org/10.1002/adma.201300923

[94] Quan, L. N., Ma, D., Zhao, Y., Voznyy, O., Yuan, H., Bladt, E., ..., & Sargent, E. H. (2020). Edge stabilization in reduced-dimensional perovskites. *Nature Communications*, *11*(1), 170. https://doi.org/10.1038/s41467-019-13944-2

[95] Zhang, D., Fu, Y., Zhan, H., Zhao, C., Gao, X., Qin, C., & Wang, L. (2022). Suppressing thermal quenching via defect passivation for efficient quasi-2D perovskite light-emitting diodes. *Light: Science & Applications*, *11*(1), 69. https://doi.org/10.1038/s41377-022-00761-4

[96] Wang, L., Shi, Z., Ma, Z., Yang, D., Zhang, F., Ji, X., ..., & Shan, C. (2020). Colloidal synthesis of ternary copper halide nanocrystals for high-efficiency deep-blue light-emitting diodes with a half-lifetime above 100 h. *Nano Letters*, *20*(5), 3568–3576. https://doi.org/10.1021/acs.nanolett.0c00513

[97] Chih, Y.-K., Wang, J.-C., Yang, R.-T., Liu, C.-C., Chang, Y.-C., Fu, Y.-S., ..., & Guo, T.-F. (2016). NiO_x electrode interlayer and $CH_3NH_2/CH_3NH_3PbBr_3$ interface treatment to markedly advance hybrid perovskite-based light-emitting diodes. *Advanced Materials*, *28*(39), 8687–8694. https://doi.org/10.1002/adma.201602974

[98] Han, P., & Zhang, Y. (2024). Recent advances in carbazole-based self-assembled monolayer for solution-processed optoelectronic devices. *Advanced Materials*, *36*(33), 2405630. https://doi.org/10.1002/adma.202405630

[99] Chu, Z., Zhao, Y., Ma, F., Zhang, C.-X., Deng, H., Gao, F., ..., & You, J. (2020). Large cation ethylammonium incorporated perovskite for efficient and spectra stable blue light-emitting diodes. *Nature Communications*, *11*(1), 4165. https://doi.org/10.1038/s41467-020-17943-6

[100] Yang, X., Chu, Z., Meng, J., Yin, Z., Zhang, X., Deng, J., & You, J. (2019). Effects of organic cations on the structure and performance of quasi-two-dimensional perovskite-based light-emitting diodes. *The Journal of Physical Chemistry Letters*, *10*(11), 2892–2897. https://doi.org/10.1021/acs.jpclett.9b00910

[101] Zhang, L., Li, N., Liu, D., Tao, G., Xu, W., Li, M., ..., & Wang, J. (2022). Deep learning for additive screening in perovskite light-emitting diodes. *Angewandte Chemie International Edition*, *61*(37), e202209337. https://doi.org/10.1002/anie.202209337

[102] Tong, G., Chen, T., Li, H., Qiu, L., Liu, Z., Dang, Y., ..., & Qi, Y. (2019). Phase transition induced recrystallization and low surface potential barrier leading to 10.91%-efficient $CsPbBr_3$ perovskite solar cells. *Nano Energy*, *65*, 104015. https://doi.org/10.1016/j.nanoen.2019.104015

[103] Li, W.-L., Hou, C.-H., Yang, C.-M., Tsai, K.-W., Wu, J.-L., Hsiao, Y.-T., ..., & Chang, Y.-M. (2021). Perfluorinated ionomer and poly(3,4-ethylenedioxythiophene) colloid as a hole transporting layer for optoelectronic devices. *Journal of Materials Chemistry A*, *9*(33), 17967–17977. https://doi.org/10.1039/D1TA04362E

[104] Lee, S. Y., Kim, S.-H., Nam, Y. S., Yu, J. C., Lee, S., Kim, D. B., ..., & Song, M. H. (2019). Flexibility of semitransparent perovskite light-emitting diodes investigated by tensile properties of the perovskite layer. *Nano Letters*, *19*(2), 971–976. https://doi.org/10.1021/acs.nanolett.8b04200

[105] Li, P., Sun, K., & Ouyang, J. (2015). Stretchable and conductive polymer films prepared by solution blending. *ACS Applied Materials & Interfaces*, *7*(33), 18415–18423. https://doi.org/10.1021/acsami.5b04492

[106] Zhang, K., Yu, S., Tu, P., Cai, X., Zhou, Y., & Mei, F. (2022). Optoelectronic properties of $MAPbBr_3$ perovskite light-emitting diodes using anti-solvent and PEDOT:PSS/PVK double-layer hole transport layers. *Micromachines*, *13*(12), 2122. https://doi.org/10.3390/mi13122122

[107] Qi, H., Wang, H., Chen, Y., Zhang, L., Wu, J., Li, T., ..., & Tong, Y. (2024). Synchronous optimization of light outcoupling and carrier recombination for efficient and spectral stable blue perovskite light-emitting diodes. *Advanced Functional Materials*, *34*(28), 2400052. https://doi.org/10.1002/adfm.202400052

[108] Yu, X., Liu, T., Wei, Q., Liang, C., Wang, K., Guo, J., ..., & Xing, G. (2020). Tailoring the surface morphology and phase distribution for efficient perovskite electroluminescence. *The Journal of Physical Chemistry Letters*, *11*(15), 5877–5882. https://doi.org/10.1021/acs.jpclett.0c01252

[109] Qin, C., Matsushima, T., Potscavage, W. J., Sandanayaka, A. S. D., Leyden, M. R., Bencheikh, F., ..., & Adachi, C. (2020). Triplet management for efficient perovskite light-emitting diodes. *Nature Photonics*, *14*(2), 70–75. https://doi.org/10.1038/s41566-019-0545-9

[110] Xiao, Z., Kerner, R. A., Tran, N., Zhao, L., Scholes, G. D., & Rand, B. P. (2019). Engineering perovskite nanocrystal surface termination for light-emitting diodes with external quantum efficiency exceeding 15%. *Advanced Functional Materials*, *29*(11), 1807284. https://doi.org/10.1002/adfm.201807284

[111] Wang, Y., Liang, Q., Huang, J., Ma, D., & Jiao, Y. (2017). Investigation of the hole transport characterization and mechanisms in co-evaporated organic semiconductor mixtures. *RSC Advances*, *7*(45), 28494–28498. https://doi.org/10.1039/C7RA05131J

[112] Yuan, S., Han, B., Fang, T., Shan, Q., & Song, J. (2020). Flat, luminescent, and defect-less perovskite films on PVK for light-emitting diodes with enhanced efficiency and stability. *ACS Applied Electronic Materials*, *2*(11), 3530–3537. https://doi.org/10.1021/acsaelm.0c00569

[113] Lee, S., Kim, D. B., Hamilton, I., Daboczi, M., Nam, Y. S., Lee, B. R., ..., & Song, M. H. (2018). Control of interface defects for efficient and stable quasi-2D perovskite light-emitting diodes using nickel oxide hole injection layer. *Advanced Science*, *5*(11), 1801350. https://doi.org/10.1002/advs.201801350

[114] Shi, Z., Li, S., Li, Y., Ji, H., Li, X., Wu, D., ..., & Du, G. (2018). Strategy of solution-processed all-inorganic

heterostructure for humidity/temperature-stable perovskite quantum dot light-emitting diodes. *ACS Nano*, *12*(2), 1462–1472. https://doi.org/10.1021/acsnano.7b07856

[115] Shen, X., Kang, K., Yu, Z., Jeong, W. H., Choi, H., Park, S. H., . . . , & Lee, B. R. (2023). Passivation strategies for mitigating defect challenges in halide perovskite light-emitting diodes. *Joule*, *7*(2), 272–308. https://doi.org/10.1016/j.joule.2023.01.008

[116] Bao, X., Gao, Y., Liu, Y., Xu, Z., Zhang, F., Lu, M., . . . , & Bai, X. (2023). Molecular bridging strategy enables high performance and stable quasi-2D perovskite light-emitting devices. *ACS Energy Letters*, *8*(2), 1018–1025. https://doi.org/10.1021/acsenergylett.2c02877

[117] Rolston, N., Watson, B. L., Bailie, C. D., McGehee, M. D., Bastos, J. P., Gehlhaar, R., . . . , & Dauskardt, R. H. (2016). Mechanical integrity of solution-processed perovskite solar cells. *Extreme Mechanics Letters*, *9*, 353–358. https://doi.org/10.1016/j.eml.2016.06.006

[118] Li, Y., Li, F., Yu, Z., Tamilavan, V., Oh, C.-M., Jeong, W. H., . . . , & Park, S. H. (2024). Effective small organic molecule as a defect passivator for highly efficient quasi-2D perovskite light-emitting diodes. *Small*, *20*(23), 2308847. https://doi.org/10.1002/smll.202308847

[119] Zhang, L., Hu, S., Guo, M., Ren, Y., Wei, L., Li, W., . . . , & Liu, B. (2023). Manipulation of charge dynamics for efficient and bright blue perovskite light-emitting diodes with chiral ligands. *Advanced Materials*, *35*(38), 2302059. https://doi.org/10.1002/adma.202302059

[120] Lee, S., Kim, D. B., Yu, J. C., Jang, C. H., Park, J. H., Lee, B. R., & Song, M. H. (2019). Versatile defect passivation methods for metal halide perovskite materials and their application to light-emitting devices. *Advanced Materials*, *31*(20), 1805244. https://doi.org/10.1002/adma.201805244

[121] Veldhuis, S. A., Boix, P. P., Yantara, N., Li, M., Sum, T. C., Mathews, N., & Mhaisalkar, S. G. (2016). Perovskite materials for light-emitting diodes and lasers. *Advanced Materials*, *28*(32), 6804–6834. https://doi.org/10.1002/adma.201600669

[122] Schmidt, I., Olthof, S., Xu, H., & Meerholz, K. (2022). Phosphine oxide additives for high-brightness inorganic perovskite light-emitting diodes. *Advanced Optical Materials*, *10*(3), 2101602. https://doi.org/10.1002/adom.202101602

[123] Zhu, C., Yuan, F., Liu, X., Li, J., Dong, H., Zhao, C., . . . , & Wu, Z. (2021). High triplet energy level molecule enables highly efficient sky-blue perovskite light-emitting diodes. *The Journal of Physical Chemistry Letters*, *12*(48), 11723–11729. https://doi.org/10.1021/acs.jpclett.1c03518

[124] Liu, L., Bi, H., Yan, J., Wang, M., & Wang, J. (2024). Defect passivation strategies in two-dimensional organic–inorganic hybrid perovskites for enhanced photoelectric performance. *Advanced Optical Materials*, *12*(27), 2401058. https://doi.org/10.1002/adom.202401058

[125] Chen, Y., Chia, J. Y. H., Su, Z. C., Tay, T. E., & Tan, V. B. C. (2013). Mechanical characterization of interfaces in epoxy-clay nanocomposites by molecular simulations. *Polymer*, *54*(2), 766–773. https://doi.org/10.1016/j.polymer.2012.11.040

[126] Chou, S. Y., Ma, R. J., Li, Y. F., Zhao, F. C., Tong, K., Yu, Z. B., & Pei, Q. B. (2017). Transparent perovskite light-emitting touch-responsive device. *ACS Nano*, *11*(11), 11368–11375. http://doi.org/10.1021/acsnano.7b05935

[127] Lu, J., Guan, X., Li, Y., Lin, K., Feng, W., Zhao, Y., . . . , & Wei, Z. (2021). Dendritic $CsSnI_3$ for efficient and flexible near-infrared perovskite light-emitting diodes. *Advanced Materials*, *33*(44), 2104414. https://doi.org/10.1002/adma.202104414

[128] Wong-Stringer, M., Game, O. S., Smith, J. A., Routledge, T. J., Alqurashy, B. A., Freestone, B. G., . . . , & Lidzey, D. G. (2018). High-performance multilayer encapsulation for perovskite photovoltaics. *Advanced Energy Materials*, *8*(24), 1801234. https://doi.org/10.1002/aenm.201801234

[129] Gu, Z., Huang, Z., Hu, X., Wang, Y., Li, L., Li, M., & Song, Y. (2020). In situ inkjet printing of the perovskite single-crystal array-embedded polydimethylsiloxane film for wearable light-emitting devices. *ACS Applied Materials & Interfaces*, *12*(19), 22157–22162. https://doi.org/10.1021/acsami.0c04131

How to Cite: Han, Q., Han, P., Wang, D., & Zhang, Y. (2025). Recent Advances in Flexible Perovskite Light-Emitting Diodes. *Smart Wearable Technology*, *1*, A8. https://doi.org/10.47852/bonviewSWT52026191